SINGLE-WALLED CARBON NANOTUBE NETWORKS: PURIFICATION, LIQUID DEPOSITION METHODS, AND MORPHOLOGICAL CONTROL ON PATTERN FORMATION

by

DOVIE MAI STANLEY

(Under the Direction of Marcus D. Lay)

ABSTRACT

A solution-based deposition technique has been proposed to allow easily for the fabrication of SWNT thin films via 2D random networks. This simple technique combines controlled evaporative and convective assembly. Moreover, it has been shown to control network density. A systematic study has been performed to gain novel knowledge about SWNT as a possible electronic material for technological applications. The study included factors that have been observed for their influence on SWNT suspension, approaches for optimizing deposition methods, and deposition methods that explored the SWNT density, network morphology, and nanotube placement.

INDEX WORDS: Single-walled carbon nanotube (SWNT) network, laminar flow deposition (LFD), network density, coffee-ring array, random network

SINGLE-WALLED CARBON NANOTUBE NETWORKS: PURIFICATION, LIQUID DEPOSITION METHODS, AND MORPHOLOGICAL CONTROL ON PATTERN FORMATION

by

DOVIE MAI STANLEY

BA, Emory University, 2005

A Dissertation Submitted to the Graduate Faculty of The University of Georgia in Partial Fulfillment of the Requirements for the Degree

DOCTOR OF PHILOSOPHY

ATHENS, GEORGIA

2016

SINGLE-WALLED CARBON NANOTUBE NETWORKS: PURIFICATION, LIQUID DEPOSITION METHODS, AND MORPHOLOGICAL CONTROL ON PATTERN FORMATION

by

DOVIE MAI STANLEY

Major Professor:	Marcus D. Lay
Committee:	John L. Stickney
	Zhangwei Pan

Electronic Version Approved:

Suzanne Barbour
Dean of the Graduate School
The University of Georgia
May 2016

TO MY PARENTS AND GRANDMOTHER

ACKNOWLEDGEMENTS

I would like to express my deepest gratitude to my committee major professor, Dr. Stickney, and Dr. Pan for your support toward my victory over this daunting process. To Dr. Stickney and Dr. Amster, your presences have been a great help, during the absence of my advisor. To my laboratory mates, I greatly appreciate everyone for sharing your lives and hearts with me as we celebrate achievements, while other times we persevere through many challenges together. To my wonderful Athens SGI family, you all have treated me like your family member by always being warm-hearted and providing me nourishment. To Ikeda, Edward, Chanda and Nichiren, your encouragements definitely made this victory possible. Finally, I will never forget the love and care of my other siblings (Stacey, Momo, Jessica, Sam, Robert, Sierra, David, and Erica), nieces/nephews, past roommates (Claudia, Pender, and Frank), other friends, and past co-workers.

TABLE OF CONTENTS

Page

LIST OF TABLES

Page

LIST OF FIGURES

Page

CHAPTER 1

INTRODUCTION AND LITERATURE REVIEW

1.1 Introduction An allotrope of carbon in which the atoms are arranged in closed shells, C_{60} or buckyball was found in 1985 by Harold W. Kroto et al.[1] Fullerenes are the groups of carbons that are connected together to form a spherical structure. The number of hexagons determines the sizes of these molecules. The carbon atoms are sp^2 and sp^3 hybridized. Within the fullerene, the sp^2 carbons are responsible for the considerably angle strain presented within the molecule.

Since the discovery of fullerenes, structural variations have evolved beyond the buckyball clusters. One variation in particular is carbon nanotubes (CNTs). A sheet of graphene rolled into a cylindrical tube, CNTs have a diameter in range of nanometers. They resemble a mesh made with hexagons of carbons. These were reported first by Iijima in 1991 when he discovered multi-walled carbon nanotubes (MWNTs), which comprise an array of tubes that are within one another like rings of a tree trunk.[2] Later, he, then, made the observation of single-walled nanotubes (SWNTs).[3] Since his discoveries, an extensively amount of work has been done over the past decades. In particularly, SWNTs have been interesting since their cylindrical shape may offer many advantageous properties.[4-6] Because of their electronic properties, SWNTs can provide the opportunity to develop new products for areas such as supercapacitors[7], field emission displays[8], and molecular computers[9].

In order to create such devices, further advancement in SWNT technology is needed. In this chapter, SWNT structure, electronic properties, SWNT synthesis, purification methods, and processing techniques for 2-dimensional (2D) assembly are explained thoroughly, and the major problems relating to each subject are also included. Finally, an overview of the work about tackling these problems is presented.

1.2 Structural and Electronic Properties of SWNTs A single-walled carbon nanotube is a graphene sheet rolled over into a cylinder, similarly to the C_{60} buckyball. SWNT has a molecular scale wire that has two structural parameters. Rolling over the lattice into a cylinder so that the beginning and end of a lattice vector in the graphene plane join together. A nanotube has formed with (m,n) indices. These indices determine the diameter of the nanotube and the chirality. When the atoms of carbon around the circumference in an armchair configuration, these (m,m) tubes are called armchair tubes. When there are (m,0) nanotubes, these tubes are called zigzag in the view of the atomic configuration along the circumference. Other types of tubes are chiral with the rows of hexagons spiraling along the nanotube axes (Figure 1.1).

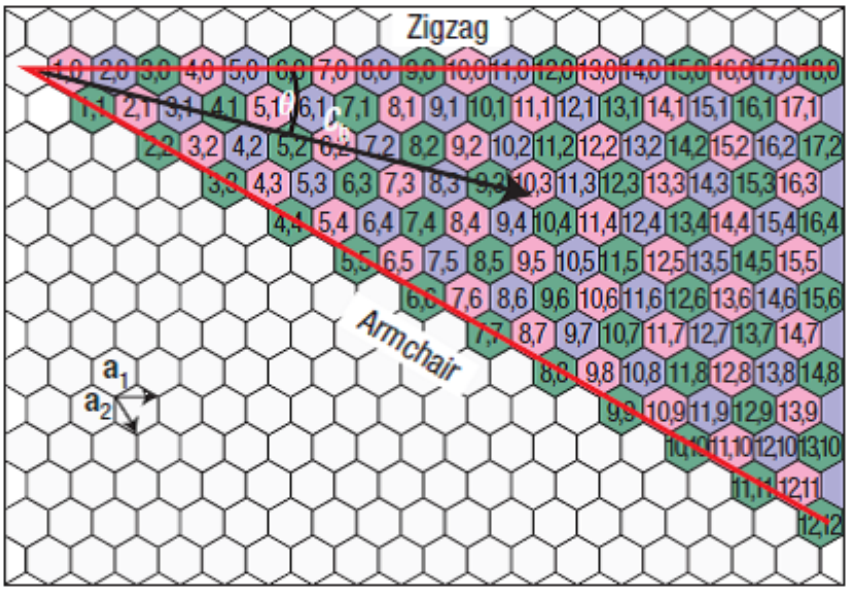

Figure 1.1. Rows of hexagons roll up along the nanotube axes to form a SWNT. Circumference of SWNT is determined by m,n indices. [10]

Because the SWNT structure influences its electronic properties, one amazing characteristic of SWNTs is that they can be metallic or semi-conducting. Research about their electronic properties is a dynamically changing field. Nevertheless, this section discusses only a brief summary of the theory of its electronic properties. Drawing on the early works of Mildred Dresselhaus et al, the band structures of three SWNT structures can now be classified simply.[11,12] The band structure of SWNTs is derived from limited number of allowed electron states in the circumferential direction. Thus, the armchair nanotubes are all metallic, while only approximately one-third of zigzag and chiral nanotubes are metallic. The remainder is semi-conducting. Another factor that can influence band structure is tube curvature. Usually having small diameters, the curvature of SWNTs is expected to introduce sp^3 character into the bonding. This causes no effect for the armchair nanotubes. However, for zigzag and chiral nanotubes that are metallic, a

band gap can form in the magnitude of $1/d^2$, where d is the diameter of the nanotube.[13] Also, in theory, the conduction and valence bands can be distorted as well.

The limited number of electronic states for SWNTs has affected also the behavior of SWNT electron transport. Starting with metallic nanotubes, their conduction happens through well separated, discrete electron states. Therefore, the resistance does not increase as the length of tube increases, without scattering. This means that long nanotubes can be used to integrate different components of a nanodevice without building resistance. Another aspect of electron transport for metallic nanotubes is its ballistic nature. The electrons encounter no resistance and dissipate no energy without scattering from impurities or phonons as they pass along the nanotube. Hence, these nanotubes can conduct a large current without becoming hot. This is a highly desirable characteristic for nano-devices! As for the semi-conducting nanotubes, scanning tunneling spectroscopy experiments have verified that the band gap decreases as the diameter of the tubes increases.[14,15] However, there have been evidence that high mobility exist in semiconducting nanotubes.[16,17] Yet, questions regarding the transport properties of semi-conducting nanotubes still exist.

Many studies have been done about the understanding in electronic properties of SWNTs and the creation of SWNT-based electronic devices. Some landmarks that are worth mentioning are the direct link to SWNT structure with its electronic properties, quantum transport, and construction of the SWNT field-effect transistors.[15,18,19] Although these have been great achievements, commercial devices are still distant options. The issues such as preparation of SWNTs and constructing a reliable arrangement for realistic applications are problems that will be addressed in later sections of this literature review.

1.3 Synthesis of SWNTs There are three main ways that the nanotubes are fabricated arc-discharge, laser ablation, and chemical vapor deposition (CVD). Here, their syntheses and growth mechanisms are described in detail. For the growth of SWNTs, a metal catalyst is needed in the arc-discharge process. The first success using this method was by Iijima et al and Bethune et al.[3,20] The optimization of SWNT growth was achieved by Journet et al using a carbon anode containing 1.0 at% of yttrium and 4.2 at. % of nickel as catalysts[21] (Figure 1.2).

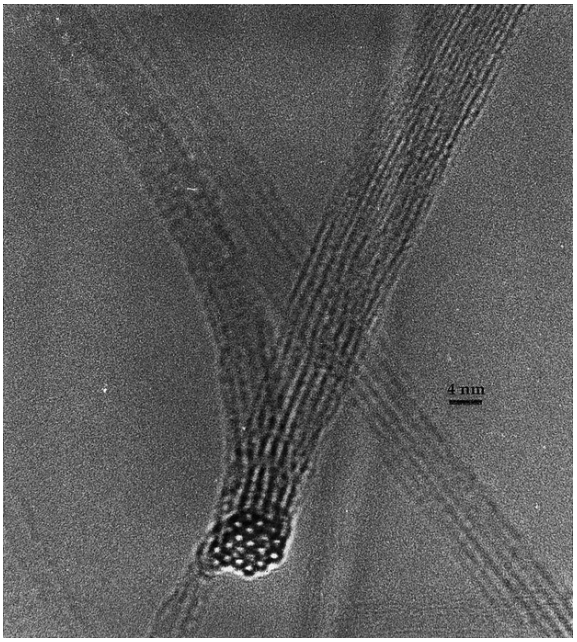

Figure 1.2. High resolution TEM image of a bundle. It is bent in such a way that it is seen edge-on. The bundle of SWNTs has a nearly uniform width of 1.4 nm and comprises approximately 20 tubes.[21]

This French group achieved high yields of 70 - 90 % and diameters of 1.4 nm, unlike to the original technique of Bethune et al that used a slightly different reactor geometry and cobalt as the promoter with diameters of 1.2 nm (Figure 1.3). Referring to a previous section, C_{60} was first discovered in 1985 as a result of experiments of the vaporization of

graphite using a Nd:YAG laser. A high quality of SWNTs was achieved by Thess et al using a laser ablation method.[23] Although laser ablation method has been developed to make SWNTs, the high cost of these powerful lasers has prevented the method in becoming widely used.

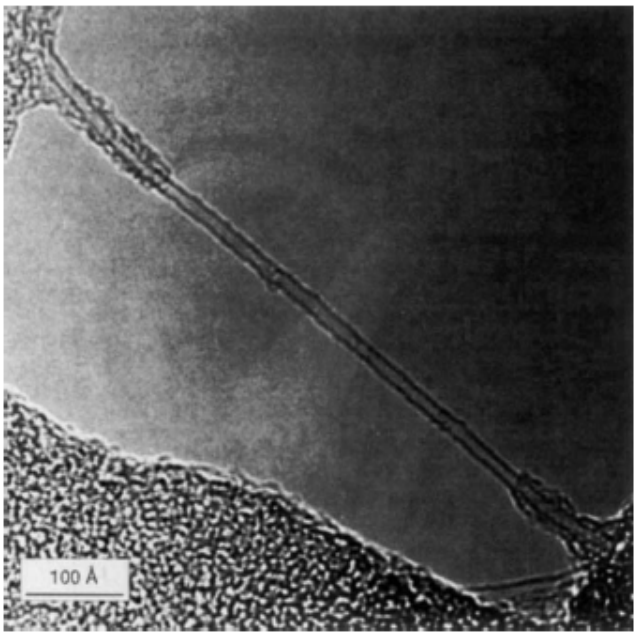

Figure 1.3. TEM image shows a bare section of a SWNT. The tube have diameters of approximately 1.2 nm.[22]

Two proposed mechanisms of SWNT synthesis in the arc-discharge and laser ablation processes are the vapor-liquid-solid (VLS) and solid-state models. Generally, it can be assumed that both processes are similar, and the mechanisms are applicable for both. Thus, both processes require sublimating graphite-metal mixture in a reduced atmosphere of inert gases. Moreover, both soot produced from the two methods are similar in appearances, containing bundles of SWNTs with amorphous carbon and metal particles. Hence, the models are accepted for both arc-discharge and laser ablation.

These models involve the nanotubes to grow away from the metal particles, and the carbon is being supplied continuously to the base. This theory is supported since most of the metal particles in the soot have diameters larger than the nanotubes and are not found at the tips of SWNTs produced by both processes. VLS, the most popular mechanism proposed, assumes that the first stage of SWNT formation starts with a condensation of carbon and meal atoms from the vapor phase to from liquid carbide particles. Then when the particles are supersaturated, the solid phase nanotubes begin to grow.[24] The driving force for the carbon nanotube growth can be either the temperature or the concentration gradients (Figure 1.4).

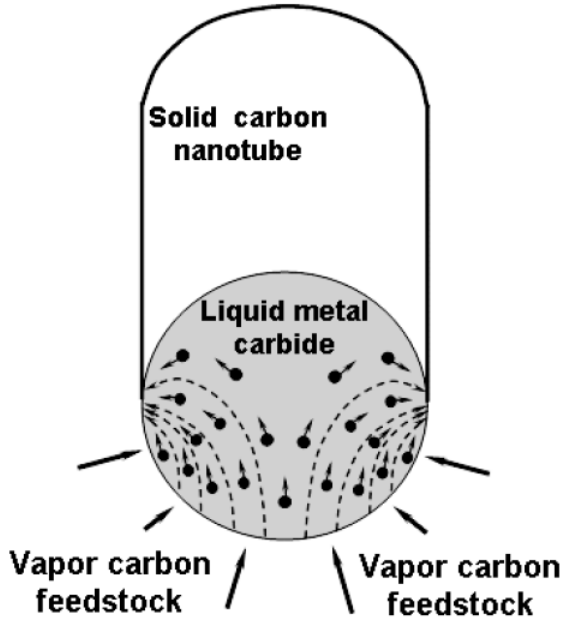

Figure 1.4. This is an illustration of the vapor-liquid-solid model. The hydrocarbons in the vapor phase react to form a liquid metal-carbide particle. This particle acts as an intermediate structure for the growth of a SWNT in a solid phase.[24]

However, other studies suggested a transformation of solid phase carbon instead of the vapor phase carbon to solid carbon tubes.[25,26] According to Geohegan et al, tube

growth did not occur during the early stages of the process when carbon in the vapor phase when growth became aggregated clusters and nanoparticles.[25] Using a Nd:YAG laser, SWNTs were prepared by ablating he graphite/NI-Co target. The laser pulse initially produces an atomic-molecular vapor containing both carbon species and Ni/Co atoms. The plasma cools fast and the carbon condenses and forms clusters. The onset of the SWNT growth is estimated to occur at 2 ms after ablation, when both the carbon and metal atoms are in a condensed form. Thus, tube growth is a solid-state process.

Finally, since the 1970s, chemical vapor deposition (CVD) of hydrocarbon gases over metal catalysts has been a classic method to produce carbon materials such as fibers, filaments, and nanotubes.[27-30] The first successful CVD synthesis of SWNTs, however, was performed in 1996.[31] This group used CO as the feedstock to pass over a catalyst containing Mo particles that were a few nanometers in diameter, at a temperature of 1200 °C. Discoveries from this group and many others created a great interest in scale-up production for SWNT technology. As a result, many approaches were developed to synthesize bulk SWNTs using the CVD process. One of the most important methods for large-scale synthesis of SWNTs is the high-pressure CO disproportionation (HiPCO) process. This utilized $Fe(CO)_5$ as a precursor for Fe clusters for the production of SWNTs form CO at approximately 1000 °C.[32] As for the growth mechanisms of catalytically produced SWNTs, the tubes are similar in appearance to the ones made by arc and laser methods. Their diameters are on the order of 1.2 nm and are formed often in packed bundles (Figure 1.5).

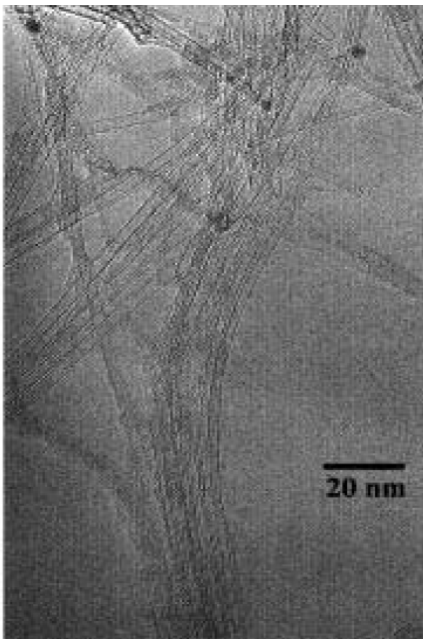

Figure 1.5. High magnification TEM image of CVD SWNTs made from FE/Mo/Al_2O_3 catalyst and CH_4.[33]

The VLS model has been assumed as the mechanism for CVD growth of SWNTs. Though the solid-state model has been shown to occur, its mechanism has not been explained.[26,34]

Despite multiple methods for SWNT growth, the quality of the tubes seems to depend less on production methods and more on post-production methods that apply these nanotubes. Arc-discharge, laser ablation, and CVD processes have produced highly flawless SWNTs that have demonstrated their excellent properties.[35-37] In addition, SWNTs from all processes can be produced in bulk. Also, advances from the CVD process have been made in SWNT growth on controlled substrates, though details about them are disclosed in a later section. Although the mechanisms of these processes are not fully understood, the VLS model is widely recognized as to be correct for all three processes. Yet, none of these produced SWNTs without nanoparticles, disordered carbon,

catalyst particles, or support materials. Therefore, it is necessary to know post-production methods to purify SWNTs without damages in order to make use of their properties.

1.4 Purification Methods In the previous section, the production processes were shown to create SWNTs that are often coated with amorphous carbon, which may be difficult to remove, as well as having relatively high percentages of amorphous carbon and metal catalysts. Purification methods that have been used are grouped into the following three categories: acid treatment and/or oxidation, functionalization, and physical techniques. Early attempts using oxidative methods proved unsuccessful since the tubes were destroyed along with the contaminants.[38-40] The source of the problem was the metal catalysts in the soot. In the presence of oxidizing gases, the metal catalysts reacted indiscriminately with carbon, thus destroying the SWNTs. Recent approaches pertaining to acid treatment and oxidation includes work by Chiang et al that describes a laser vaporization method to purify nitric acid treated SWNTs (Figure 6a).[41,42] After filtration and a series of oxidation steps, the samples were reported to contain 99.9 % SWNTs (Figure 6b).

(a) 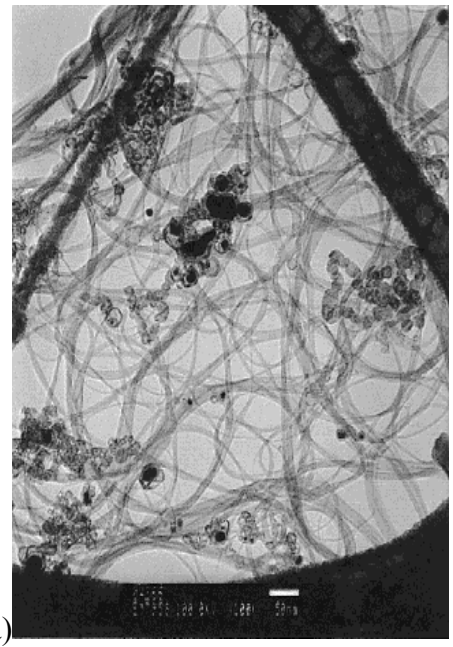 (b) 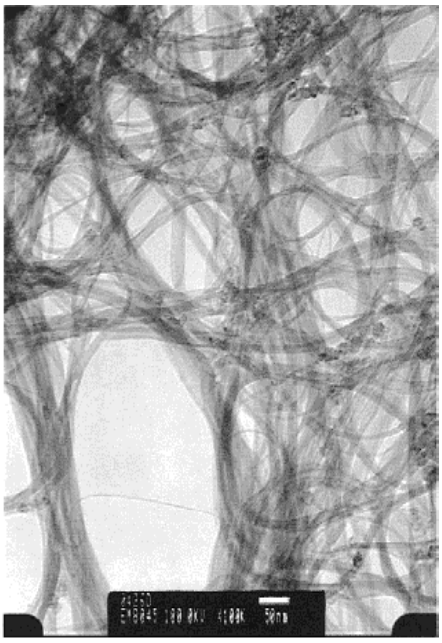

Figure 6. TEM images showing the purification of SWNTs (a) untreated soot (b) soot after the purification treatment.[41]

Yet, this type of purification must consider the formation of functional groups, especially carboxylic acid, at the ends of the tube or even on the sidewalls where they can bond at the defective sites. These functional groups may decrease the effectiveness of properties of the nanotubes.

Functionalization of the sidewalls and ends of the SWNTs is a possible purification route. In many studies, the purpose of functionalization was to make SWNTs soluble to polar environments. Moreover, this technique has proved useful for purifying SWNTs for Maurizio Prato et al.[43,44] They showed the functionalizing SWNTs with azomethine ylides could purify SWNTs produced by a gas-phase reaction of iron carbonyl with high-pressure carbon monoxide gas. Another group used ozonolysis to functionalize the sidewalls of the SWNTs.[45,46] They reported that smaller tubes were more susceptible to ozonolysis. Also, this process caused the amorphous carbon and

carbon-coated nanoparticles to functionalize heavily with the oxygenated groups. Therefore, the solubility of the amorphous carbon and nanoparticles increased in polar solvents that were used to remove them. Yet, major questions, such as the type of functional group that would provide SWNTs that have a higher purity and less damage, needs to be investigated thoroughly.

Physical techniques have been used as purification methods since they have proved to be less destructive and dangerous than chemical methods. Many types of physical techniques for the purification of SWNTs exist. They have achieved in obtaining SWNTs of precisely defined length, diameter, and chirality. Since the strength and efficacy of SWNT properties are dependents of these physical traits, it has been important to develop protocols that can remove impurities and separate nanotubes according to the desired application. In addition, for larger quantities of material for electronic devices, centrifugation offers a great option to enhance the SWNT purity. The rate of centrifugation depends on the angular velocity measured in revolutions per minute. The two types of centrifugation discussed are low-speed centrifuges and ultracentrifuges. Low-speed centrifuges can quickly change speeds and spin at maximum angular speeds of 13,000 rpm. On the other hand, ultracentrifugation requires refrigeration and has speeds that may reach 150,000 rpm. While micro-centrifuges can process separate nanotubes from impurities, ultracentrifuges can isolate even smaller particles such as SWNT length and density of nanotubes.

Despite huge efforts that have been exerted in developing techniques for purifying SWNTs, purification methods are still needed to generate undamaged, pristine nanotubes with high aspect ratios for electronic devices. Our group demonstrated that low-speed

centrifugation is a key purifying technique. It has been shown to be effective in removing amorphous carbon and catalyst nanoparticles, while leaving high-aspect-ratio SWNTs in suspension.[47] This is used since there are considerations for the types of nanotubes produced and the purpose of their applications**.** Therefore, finding a method to purify SWNTs that understands the effects of different diameters and amounts of catalysts in the soot is still a great challenge.

1.5 Techniques for SWNT Assembly SWNTs have small dimensions and excellent electronic properties that make them promising materials for nanoscale devices as previously discussed. In addition, SWNTs need to be assembled into hierarchical arrays over large areas for them to be used as transistors or sensors in these devices. Yet, the assembly of nanotubes at certain locations with desired shapes, directions, and densities for fabrication of such active components has been one of the oldest problems of SWNT technology that remains unsolved.[48-50] So, in the following section, a snapshot of the techniques, which align and pattern 2-dimensionally SWNTs either during nanotube production or post-production, is addressed. The use of nanotube production, the CVD process, provides one approach of organizing SWNTs into defined networks. As mentioned earlier, there have been advances in CVD process for SWNT growth on certain substrates. This is of particular interest since it is a one-step synthesis process for SWNT array alignment on the substrate without pretreatment of the substrate.[48,51] Many techniques have been developed to yield SWNT architectures and to promote fabrication of devices.[52-54]

Post-production methods offer an effective route for SWNT assembly. Using self-assembled monolayers of molecules on a substrate, gas flow-induced method, DNA-

template method, di-electrophoresis, and Langmuir-Blodgett technique are some ways to manipulate the alignment and arrangement of SWNTs.[55-59] Most approaches require SWNTs to be suspended in a specific solution, where the solvent can acts as a carrier and a lubricant. This SWNT suspension is made from one of the purification processes discussed earlier. The nanotubes are mobile in the solution, and the assembly takes place on the surface of a substrate that is usually smooth. Once the nanotubes are settled down on the surface, they adhere on the surface randomly, and the bond strength depends on the physical or chemical interactions between the SWNTs and the surface. Different forces such as van der Waals, hydrogen bonding, and hydrophobic forces can be used to take enhance that bond strength. Meanwhile, other techniques use external forces to drive the SWNT assembly. Shear, electric, and magnetic forces are examples of those forces that aid in SWNT alignment and patterning.

The development of the processing techniques has led many advances in the SWNT assembly. Moreover, ultimately an ideal assembly process would be cost-efficient, reliable, and capable to direct the SWNT placement over a large area substrate easily. When choosing a feasible method for fabrication of nanoscale devices, the production approach, CVD process, has two main limitations over the post-production approach. Its approach is limited to only a few types of materials and relatively simple structures. Whereas post-production techniques offer ways to assemble SWNTs into complex architectures on any desired substrate, and thus, these techniques are more flexible for fabrication. However, further research on post-production techniques is still needed to improve on the process reproducibility and reliability.

1.6 Scope of The Research Being a great interest to scientists, earlier works mentioned have set the foundation for SWNT technology. Areas discussed are its structure and electronic properties, synthesis of long and nearly perfect nanotubes, purification processes that remove the impurities, and SWNT assembly techniques for device fabrication. These are areas of great importance in SWNT technology since they increase the knowledge needed for the commercial use of SWNTs. However, problems with purification and SWNT assembly still exist. So, an understanding of how to manipulate SWNTs during the purification process and assembly is necessary. Thus, leading this research is finding ways to understand and to predict the behavior of SWNTs in 2D networks for use in electronic materials.

In the second chapter, understanding the effects of the starting concentration of unprocessed SWNTs using low-G force centrifugation was studied to overcome the challenge of predicting SWNT network properties at ambient conditions. Enabling SWNTs to assemble into materials that make use of their enhanced properties in electronics and nanotechnology requires purification of these nanotubes. Different concentrations of SWNT suspensions were analyzed to show their influences on the SWNT density, the network morphology, and the placement of the SWNT networks on Si/SiOx substrates. Then, the third chapter explores controlled evaporative methods to control SWNT assembly. Taking advantage of a natural phenomenon, the coffee-ring effect (CR) offers a simple and inexpensive way to assemble SWNT networks with the assistance of laminar flow deposition process. Thus, using the CR, the study compared the spatial and temporal differences of two incubation methods, immerse and drop. In the fourth chapter, 2D network formation using the CR deposition was studied as a possible

approach for assembling SWNT devices. The interactions between different self-assembled monolayers of vinyl silanes on Si/SiOx substrates and starting concentrations of unprocessed SWNTs determined the parameters of the network formation process. Moreover, this method demonstrated a potential route for controlling the level of randomness and order of the 2D SWNT networks. Lastly, the final chapter summarizes achievements and proposes future works in SWNT research.

1.7 References

1 Kroto, H. W., Heath, J. R., O'Brien, S. C., Curl, R. F. & Smalley, R. E. C 60: buckminsterfullerene. *Nature* **318**, 162-163 (1985).

2 Iijima, S. Helical microtubules of graphitic carbon. *nature* **354**, 56-58 (1991).

3 Iijima, S. & Ichihashi, T. Single-shell carbon nanotubes of 1-nm diameter. (1993).

4 Cornwell, C. & Wille, L. Elastic properties of single-walled carbon nanotubes in compression. *Solid State Communications* **101**, 555-558 (1997).

5 Issi, J. P., Langer, L., Heremans, J. & Olk, C. Electronic properties of carbon nanotubes: Experimental results. *Carbon* **33**, 941-948 (1995).

6 Rosen, R. *et al.* Application of carbon nanotubes as electrodes in gas discharge tubes. *Applied physics letters* **76**, 1668-1670 (2000).

7 An, K. H. *et al.* in *AIP Conference Proceedings*. 241.

8 Choi, W. *et al.* Fully sealed, high-brightness carbon-nanotube field-emission display. *Applied physics letters* **75**, 3129-3131 (1999).

9 Rueckes, T. *et al.* Carbon nanotube-based nonvolatile random access memory for molecular computing. *Science* **289**, 94-97 (2000).

10 Li, H. & Li, Q. *Selective Separation of Single-Walled Carbon Nanotubes in Solution*. (2011).

11 Dresselhaus, M., Dresselhaus, G. & Saito, R. Physics of carbon nanotubes. *Carbon* **33**, 883-891 (1995).

12 Saito, R., Fujita, M., Dresselhaus, G. & Dresselhaus, u. M. Electronic structure of chiral graphene tubules. *Applied physics letters* **60**, 2204-2206 (1992).

13 Ouyang, M., Huang, J.-L., Cheung, C. L. & Lieber, C. M. Energy gaps in" metallic" single-walled carbon nanotubes. *Science* **292**, 702-705 (2001).

14 Odom, T. W., Huang, J.-L., Kim, P. & Lieber, C. M. Atomic structure and electronic properties of single-walled carbon nanotubes. *Nature* **391**, 62-64 (1998).

15 Wilder, J. W., Venema, L. C., Rinzler, A. G., Smalley, R. E. & Dekker, C. Electronic structure of atomically resolved carbon nanotubes. *Nature* **391**, 59-62 (1998).

16 Martel, R., Schmidt, T., Shea, H., Hertel, T. & Avouris, P. Single-and multi-wall carbon nanotube field-effect transistors. *Applied Physics Letters* **73**, 2447-2449 (1998).

17 Dürkop, T., Getty, S., Cobas, E. & Fuhrer, M. Extraordinary mobility in semiconducting carbon nanotubes. *Nano letters* **4**, 35-39 (2004).

18 Tans, S. J. *et al.* Individual single-wall carbon nanotubes as quantum wires. *Nature 386 (6624), 474-477.(1997)* (1997).

19 Tans, S. J., Verschueren, A. R. & Dekker, C. Room-temperature transistor based on a single carbon nanotube. *Nature* **393**, 49-52 (1998).

20 Bethune, D. *et al.* Cobalt-catalysed growth of carbon nanotubes with single-atomic-layer walls. (1993).

21 Journet, C. *et al.* Large-scale production of single-walled carbon nanotubes by the electric-arc technique. *nature* **388**, 756-758 (1997).

22 Bethune, D. S. *et al.* Cobalt-catalysed growth of carbon nanotubes with single-atomic-layer walls. *Nature* **363**, 605-607 (1993).

23 Thess, A. *et al.* Crystalline ropes of metallic carbon nanotubes. *Science-AAAS-Weekly Paper Edition* **273**, 483-487 (1996).

24 Bolton, K., Ding, F. & Rosén, A. Atomistic simulations of catalyzed carbon nanotube growth. *Journal of nanoscience and nanotechnology* **6**, 1211-1224 (2006).

25 Geohegan, D. *et al.* Condensed phase growth of single-wall carbon nanotubes from laser annealed nanoparticulates. *Applied Physics Letters* **78**, 3307-3309 (2001).

26 Gorbunov, A., Jost, O., Pompe, W. & Graff, A. Solid–liquid–solid growth mechanism of single-wall carbon nanotubes. *Carbon* **40**, 113-118 (2002).

27 Baker, R. Catalytic growth of carbon filaments. *Carbon* **27**, 315-323 (1989).

28 Tibbetts, G. G., Meisner, G. P. & Olk, C. H. Hydrogen storage capacity of carbon nanotubes, filaments, and vapor-grown fibers. *Carbon* **39**, 2291-2301 (2001).

29 Baker, R., Barber, M., Harris, P., Feates, F. & Waite, R. Nucleation and growth of carbon deposits from the nickel catalyzed decomposition of acetylene. *Journal of catalysis* **26**, 51-62 (1972).

30 Kong, J., Soh, H. T., Cassell, A. M., Quate, C. F. & Dai, H. Synthesis of individual single-walled carbon nanotubes on patterned silicon wafers. *Nature* **395**, 878-881 (1998).

31 Dai, H. *et al.* Single-wall nanotubes produced by metal-catalyzed disproportionation of carbon monoxide. *Chemical Physics Letters* **260**, 471-475 (1996).

32 Nikolaev, P. *et al.* Gas-phase catalytic growth of single-walled carbon nanotubes from carbon monoxide. *Chemical physics letters* **313**, 91-97 (1999).

33 Cassell, A. M., Raymakers, J. A., Kong, J. & Dai, H. Large scale CVD synthesis of single-walled carbon nanotubes. *The Journal of Physical Chemistry B* **103**, 6484-6492 (1999).

34 Sen, R., Suzuki, S., Kataura, H. & Achiba, Y. Growth of single-walled carbon nanotubes from the condensed phase. *Chemical physics letters* **349**, 383-388 (2001).

35 An, K. H. *et al.* Electrochemical properties of high-power supercapacitors using single-walled carbon nanotube electrodes. *Advanced functional materials* **11**, 387-392 (2001).

36 Cheung, C. L., Hafner, J. H., Odom, T. W., Kim, K. & Lieber, C. M. Growth and fabrication with single-walled carbon nanotube probe microscopy tips. *Applied Physics Letters* **76**, 3136-3138 (2000).

37 Sakakibara, Y., Tatsuura, S., Kataura, H., Tokumoto, M. & Achiba, Y. Near-infrared saturable absorption of single-wall carbon nanotubes prepared by laser ablation method. *Japanese journal of applied physics* **42**, L494 (2003).

38 Dujardin, E., Ebbesen, T., Hiura, H. & Tanigaki, K. Capillarity and wetting of carbon nanotubes. *Science* **265**, 1850-1852 (1994).

39 Hiura, H., Ebbesen, T. W. & Tanigaki, K. Opening and purification of carbon nanotubes in high yields. *Advanced materials* **7**, 275-276 (1995).

40 Dujardin, E., Ebbesen, T. W., Krishnan, A. & Treacy, M. M. J. Purification of single-shell nanotubes. *Advanced materials* **10**, 611-613 (1998).

41 Chiang, I. *et al.* Purification and characterization of single-wall carbon nanotubes (SWNTs) obtained from the gas-phase decomposition of CO (HiPco process). *The Journal of Physical Chemistry B* **105**, 8297-8301 (2001).

42 Chiang, I., Brinson, B., Smalley, R., Margrave, J. & Hauge, R. Purification and characterization of single-wall carbon nanotubes. *The Journal of Physical Chemistry B* **105**, 1157-1161 (2001).

43 Georgakilas, V. *et al.* Organic functionalization of carbon nanotubes. *Journal of the American Chemical Society* **124**, 760-761 (2002).

44 Georgakilas, V. *et al.* Purification of HiPCO carbon nanotubes via organic functionalization. *Journal of the American Chemical Society* **124**, 14318-14319 (2002).

45 Banerjee, S. & Wong, S. S. Rational sidewall functionalization and purification of single-walled carbon nanotubes by solution-phase ozonolysis. *The Journal of Physical Chemistry B* **106**, 12144-12151 (2002).

46 Banerjee, S. & Wong, S. S. Demonstration of diameter-selective reactivity in the sidewall ozonation of SWNTs by resonance Raman spectroscopy. *Nano letters* **4**, 1445-1450 (2004).

47 Vichchulada, P., Shim, J. & Lay, M. D. Non-oxidizing Purification Method for Large Volumes of Long, Undamaged Single-Walled Carbon Nanotubes. *The Journal of Physical Chemistry C* **112**, 19186-19192 (2008).

48 Dai, L. *et al.* Aligned nanotubes. *ChemPhysChem* **4**, 1150-1169 (2003).

49 Liu, J. *et al.* Fullerene pipes. *Science* **280**, 1253-1256 (1998).

50 Xiang, L. *et al.* Vertically Aligned Carbon Nanotube-Sheathed Carbon Fibers as Pristine Microelectrodes for Selective Monitoring of Ascorbate in Vivo. *Analytical chemistry* **86**, 3909-3914 (2014).

51 Sugime, H., Noda, S., Maruyama, S. & Yamaguchi, Y. Multiple "optimum" conditions for Co–Mo catalyzed growth of vertically aligned single-walled carbon nanotube forests. *Carbon* **47**, 234-241 (2009).

52 Han, Z. J. *et al.* SWCNT networks on nanoporous silica catalyst support: morphological and connectivity control for nanoelectronic, gas-sensing, and biosensing devices. *ACS nano* **6**, 5809-5819 (2012).

53 Hofmann, S., Ducati, C., Kleinsorge, B. & Robertson, J. Direct growth of aligned carbon nanotube field emitter arrays onto plastic substrates. *Applied physics letters* **83**, 4661-4663 (2003).

54 Murata, K., Matsumoto, J., Tezuka, A., Matsuba, Y. & Yokoyama, H. Super-fine ink-jet printing: toward the minimal manufacturing system. *Microsystem Technologies* **12**, 2-7 (2005).

55 Li, X. *et al.* Langmuir-Blodgett assembly of densely aligned single-walled carbon nanotubes from bulk materials. *Journal of the American Chemical Society* **129**, 4890-4891 (2007).

56 Liu, Z. *et al.* Organizing single-walled carbon nanotubes on gold using a wet chemical self-assembling technique. *Langmuir* **16**, 3569-3573 (2000).

57 Maune, H. T. *et al.* Self-assembly of carbon nanotubes into two-dimensional geometries using DNA origami templates. *Nature nanotechnology* **5**, 61-66 (2010).

58 Seo, H.-W., Han, C.-S., Choi, D.-G., Kim, K.-S. & Lee, Y.-H. Controlled assembly of single SWNTs bundle using dielectrophoresis. *Microelectronic Engineering* **81**, 83-89 (2005).

59 Zhang, Q., Vichchulada, P., Cauble, M. A. & Lay, M. D. Percolation in networks of aligned SWNTs formed with laminar flow deposition. *Journal of materials science* **44**, 1206-1211 (2009).

CHAPTER 2

EFFECTS OF STARTING CONCENTRATION ON SWNT PURIFICATION PROCESS[1]

[1] Stanley, D.M. and M.D. Lay. To be submitted in J. Mat. Sci.

2.1 Abstract Assembling single-walled carbon nanotubes (SWNTs) into materials that make use of their enhanced electronic and physical properties requires new purification methods. To study the effects of initial concentration on SWNT suspensions on the purification process, as produced SWNT soot, in a range of concentrations from 0.01 to 1 mg/mL, was dispersed in sodium dodecyl sulfate via probe sonication followed by low G centrifugation steps to remove impurities. Moreover, this method enriched the suspension in regards to high-aspect-ratio SWNTs. The first centrifugal cycle removed the largest amount of sediments than any cycle. Furthermore, the UV-vis spectra showed that absorbance of the SWNT suspension have decreased from the initial absorbance for all concentrations. The removal of the sediments allowed the optical transitions of nanotubes to be observed. Additionally, NIR spectra showed that this absorbance drop seen after the first centrifugal cycle increased as the concentration increased. Then, SWNT suspensions were utilized to form 2-dimensional (2D) networks on Si/SiOx substrates via the laminar flow deposition process. The effect on SWNT density and the network morphology were analyzed. The results showed that the mean height of the SWNT network increased as the concentration of SWNTs suspension increased. For the length distribution, the length of the nanotubes increased as the number of centrifugal cycles increased. As a result, after three centrifugation cycles, the suspensions began with similar number of individual SWNTs, but the amount of nanotubes increased for all concentration after centrifugation.

2.2 Introduction Due to their enhanced electrical properties, and ability to form semiconductive or metallic thin-films, there is great interest in the use of single-walled carbon nanotubes (SWNTs) for a multitude of next generation electronic device

structures. However, regardless of the bulk growth method used for SWNTs, the product is largely composed of soot, and residual catalyst nanoparticles. These impurities often account for 40 to 60 % of as-produced (AP-grade) SWNT soot. Moreover, strong inter-SWNT van der Waals interactions cause them to clump together into bundles of hundreds of nanotubes.[1-4] Additionally, purified SWNTs are a polydisperse material, exhibiting a wide variety of bandgaps, lengths, and diameters. Individual SWNTs even exhibit metallic or semiconductive behavior, as dictated by the chirality of each nanotube. Therefore, purifying and unbundling SWNTs without damaging their electrical properties is a major focus of scientific investigation.[4-10]

One approach to dealing with the variations in electrical properties of SWNTs is the use of networks of SWNTs.[11] Such networks exhibit much greater current drive than an individual SWNT and result in greatly improved device reproducibility.[11] Additionally, these networks can serve as semiconductive thin-films with the use of methods to enrich the proportion of semiconductive SWNTs,[12] change their electrical properties via polymer or DNA wrapping,[13, 14] or control the density of SWNTs during network formation.[15] Suspension deposition methods require stable suspensions of known SWNT concentration. Thus, there is a great need for large-scale purification methods that will unbundle SWNTs and separate them from residual impurities without damaging their electrical properties.

Low-G centrifugation has been shown to be effective in removing amorphous carbon and catalyst nanoparticles, while leaving high-aspect-ratio SWNTs in suspension.[4, 9, 16] Sodium dodecyl sulfate (SDS) was chosen as the surfactant for these studies because, of the many commonly used surfactants, it has the lowest binding energy

with SWNTs of diam. ~ 1.2 nm,[17] typical of the arc discharge nanotubes used in these studies. A low surfactant binding energy is an important consideration for post-deposition removal of surfactants from the SWNT networks, as surfactant reduces their electrical performance.

In order to determine the effect of starting concentration on the average length, density and effectiveness of removing bundles, five initial concentrations were examined. These studies will allow the preparation of high quality, purified dispersions enriched in unbundled, high-aspect ratio SWNTs having minimal modification to their inherent electrical properties.

2.3 Experimental Methods

SWNT suspension formation

1 % SDS (J.T. Baker) stock solution was formed in nanopure water (R > 18.1 MΩ). Then, enough SWNT soot to yield a concentration of 1 mg/mL was dispersed in this solvent via 30 minutes of ultrasonic probe agitation (Fisher, 500) at 12 W. This stock suspension was then diluted with 1 % SDS to form the five concentrations investigated: 0.1, 0.08, 0.05, 0.03, and 0.01 mg/mL. Each suspension was mixed using a vortex after dilution (Thermolyne model 37600).

Analytical methods

UV-Vis-NIR, spectroscopy (Varian, Cary 5000) was used to characterize each suspension (path length = 1cm) over the course of three centrifuge cycles. Raman spectroscopy (ThermoFisher, DXR) was performed with a 532 nm diode laser source with 5 mW laser power. Suspensions were encapsulated in a 1.5 x 90 mm capillary tube prior to Raman analysis, while low-density SWNT networks dispersed on silicon wafer

(Si/SO_x) wafer fragments were analyzed without further modification. The SWNT networks are prepared using laminar flow deposition (LFD), a method previously described.[4, 9] Each centrifugation cycle involved a 30-minute period at 18,000 G (Beckman Microfuge18Centrifuge), after which the upper half of the supernatant carefully decanted. Finally, atomic force microscopy (AFM, Molecular Imaging, PicoPlus) was used to analyze deposits formed from each suspension to determine the differences in SWNT properties and the amount of SWNT and impurities deposited for each concentration.

2.4 Results and Discussion

UV-Vis-NIR characterization

In the previous chapter, the metallic and semiconducting behaviors of SWNTs were stated to be a function of diameter and chirality. Moreover, this was determined with discontinuous peaks in the density of states.[18] These peaks are called Van Hove singularities (VHS) and reflect the one-dimensional electronic band structure of SWNTs. Scientists have been greatly interested in VHS since the energies between them can determine the optical properties of carbon nanotubes.[3, 19] The difference of energies is also referred as a transition. It occurs between the states of semiconducting or metallic tubes and can be seen in the optical spectra. The optical transitions for semiconducting are known as S_{11} and S_{22}, while the transition for metallic is M_{11}. Furthermore, UV-Vis-NIR absorption spectroscopy is commonly used to characterize SWNT suspensions since the nanotubes have active electronic transitions in this region that give rise to van Hove singularities in the optical spectra.[20] A typical absorption spectrum shows these various peaks between 400 and 1400 nm. Peaks, due to the first interband transitions of metallic

SWNTs (M_{11}), range from 400 to 650 nm. Peaks due to the first and second interband transitions of semiconducting tubes (S_{11} and S_{22}) range from 900 to 1600 nm and 550 to 900 nm, respectively.[20-22]

In general, the absorbance for each suspension decreased inversely proportional to the number of centrifugation cycles it was subjected to (Figure 2.1). In Figure 2.1a, the initial concentrations have high absorbance and less resolution of transitional peaks. For 0.1 mg/mL, noise was seen between 200 — 400 nm region due to oversaturation of the detector. Still, in the UV region from 200-300 nm, 0.03 mg/mL and 0.01 mg/mL samples showed a broadening of the peak. Since the amounts of the impurities and SWNTs were nearly equal, there were not a clear distinction between 275 nm (the peak associated with SWNTs) and 250 nm (the peak associated with the small carbon-carbon bonds or carbonaceous materials).[23] In Figure 2.1b, after centrifugation, there were less absorbance and more resolved peaks. Such peaks were located at 275 nm as the shouldered peak of the carbonaceous peak at 250 nm and also metallic transitional peak at 750 nm. Furthermore, based on the quality of the spectra, it was concluded that a significant amount of the particles has been removed from the suspensions after the third centrifugation. The 0.1 mg/mL suspension was used to hypothesize the changes that have occurred for all other suspensions since this concentration had the strongest absorbance than the more diluted suspensions of 0.05 mg/mL and 0.03 mg/mL. Because of the low-G centrifugation, the large amount of carbonaceous matter had been separated out of the suspension. As a result, again observing the range from 200–300 nm, there was an increase of absorbance seen around 275 nm that was related to SWNTs, as well as the metallic SWNTs prominent peak.

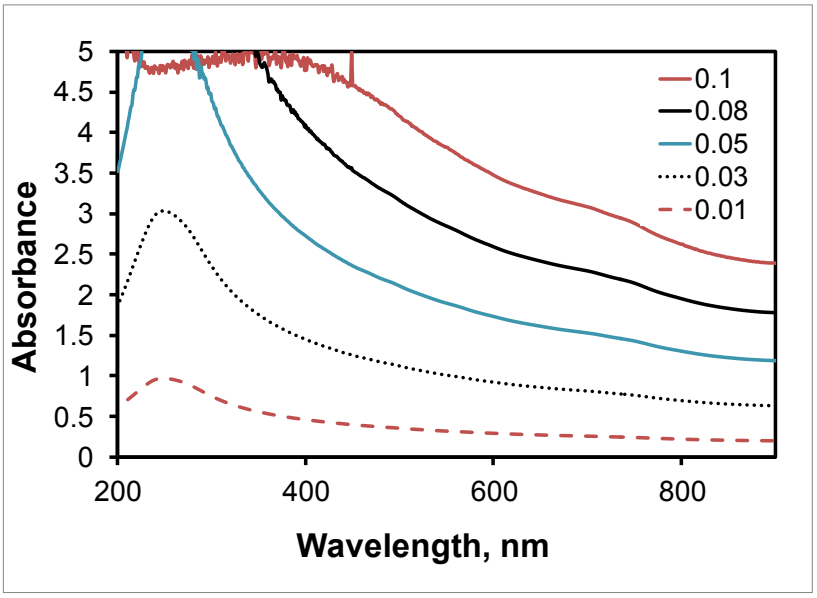

(a)

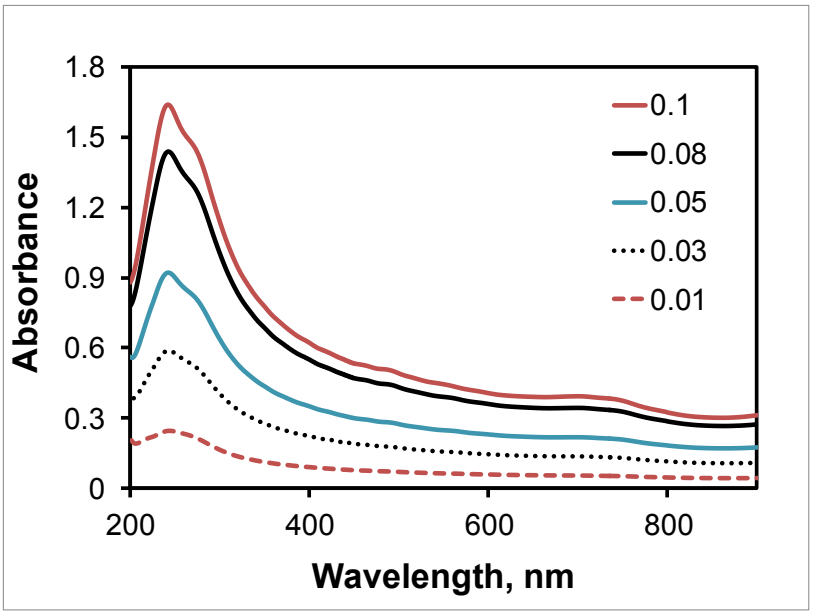

(b)

Figure 2.1. UV-Vis-NIR spectra. (a) Before centrifugation (b) After the 3rd centrifugal cycle. For 0.1 mg/mL, noises are found from 200 to 400 nm, indicating oversaturation. In addition, spectra show that SWNT Peaks at 275nm and 750nm are enhanced relative to the baseline. 275nm is associated with SWNT and 250nm peak is small c-c bonds; M_{11}-first metallic transition; S_{22} and S_{11} overlapping each other. This shows how all concentrations are related to each other.

The absorbance spectroscopy indicated that this purification method enriched the suspension in unbundled SWNTs, while removing carbonaceous impurities, as evidenced by the increased prominence and resolution of absorption bands due to unbundled SWNTs. Yet, not only was a qualitative analysis obtained but a quantitative one as well using UV-Vis-NIR spectroscopy to determine the SWNTs' purity. For determination of the concentration of SWNTs, the absorbance taken at 600 nm was used because the relationship between the concentration and absorbance (Beer's law) was more linear.[24]

Figure 2.2 showed the degree of separation of impurities from the suspension. In Figure 2.2a, the linear regression lines have larger decline in the slope between the first and second centrifugal cycle than second and third centrifugal cycles. Thus, the largest amounts of impurities and SWNT's were removed in the first cycle than the other cycles. In addition to the decrease of the slope, the increase in linearity becomes more consistent to Beer's law. This confirmed that the increasing amount of centrifugal cycles done on a suspension removes impurities from the suspension. Another observation was that suspension with a higher starting concentration removed a larger percentage of substances in the suspension. Figure 2.2b plotted the relationship between the centrifugal cycles and absorbance. After the first cycle, the suspensions leveled out, which suggested a large majority of impurities was removed after the first cycle. This was a better estimation of the relative concentration of the suspension, and more importantly, the low-G centrifugation method removed impurities from the suspensions.

(a)

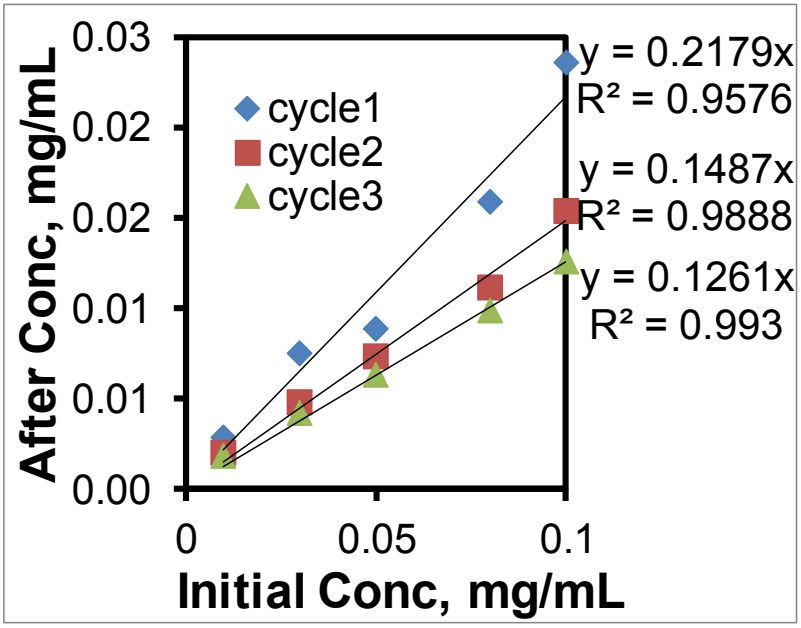

(b)

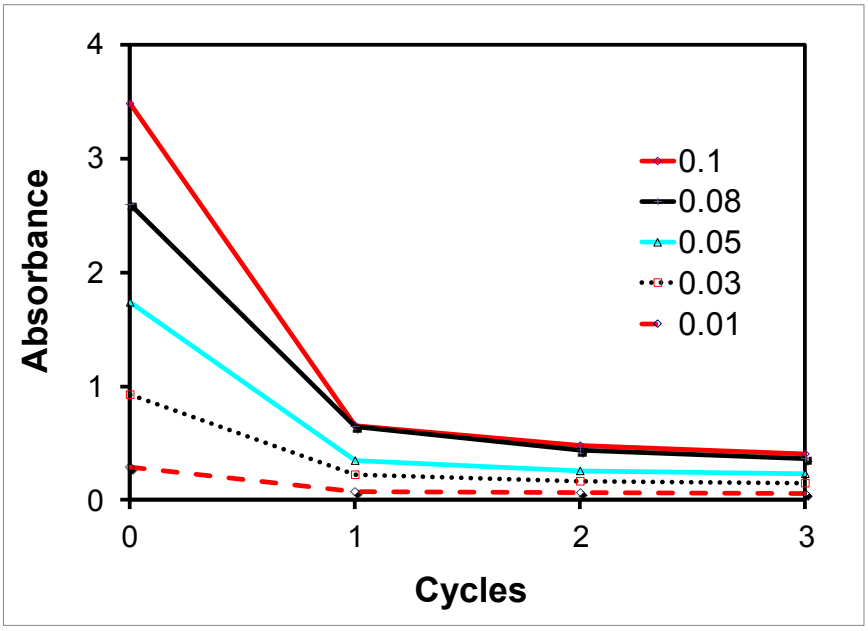

Figure 2.2. Effects of Centrifugation. (a) Concentration of each cycle (b) Absorbance after each cycle.

The NIR region is where the interband transitions are located. These bands are used to evaluate the relative purity of suspensions. In Figure 2.3a, the NIR spectra of the suspensions were taken before centrifugation. Here, the M_{11} and overlapping S_{22} and S_{11}

transitions were not well defined for any concentrations. In contrast, the NIR spectra of the purified suspensions (Figure 2.3b) showed more defined, transitional peaks for metallic and semiconducting SWNTs in each suspension, with the varying physical properties of the SWNTs contributing to the broadness of the peaks. Hence, low-G centrifugation promoted the purity of the suspensions as evidently shown in the NIR spectra.

(a)

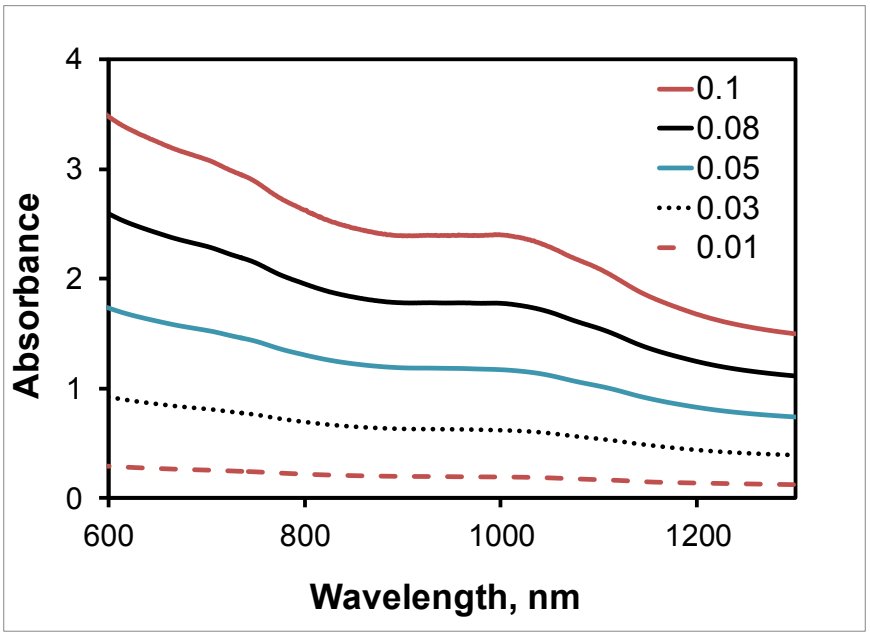

(b)

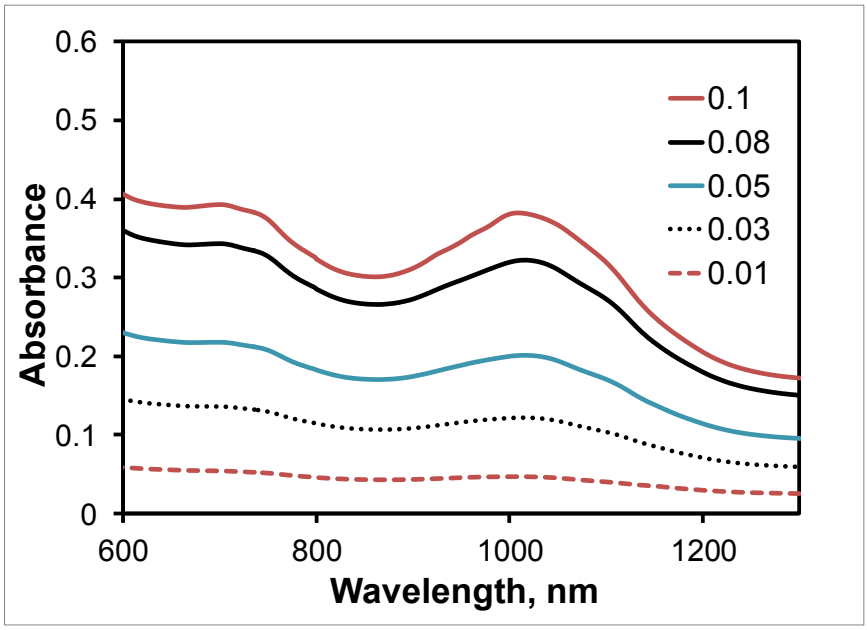

Figure 2.3. NIR spectra. (a) Suspensions before centrifugation (b) Suspensions after third centrifuge cycle. There were partial metallic transition at 800nm; 2nd semiconducting transition at 1000nm; and 1st semiconducting transition at 1100nm.

Figure 2.4a, the relationship between each suspensions normalized at the 1015 nm peak was observed. A similar broad resolution was seen; however, due to the absorption of the carbonaceous materials alongside the SWNTs, shifting could be determined. Another type of baseline correction was performed where the broad background due to π-plasmon absorbance[25] was subtracted, which left behind the transitional peaks for semiconducting SWNTs (Figure 2.4b). S_{22} peak was chosen for purity evaluation based on purity evaluation based on previous studies.[26] Then, finding the apex of the second transition peak of each suspension, only shifting of a few nanometers between the suspensions, except between 0.1 and 0.03 mg/mL, was observed. However, in both Figures 2.4a and b, besides the different area of the peaks due to the concentration and small random shifting for 0.08 mg/mL, 0.05 mg/mL, and 0.03 mg/mL, there was no

significant difference in the spectra offset. Each concentration may have represented similar ratios of SWNTs to impurities or even free SWNTs to bundled SWNTs. More studies would need to be done in order to verify this finding such as comparing the areas of the peak to different concentrations, observing any difference between the concentrations in each cycle, and comparing other techniques that have been published.

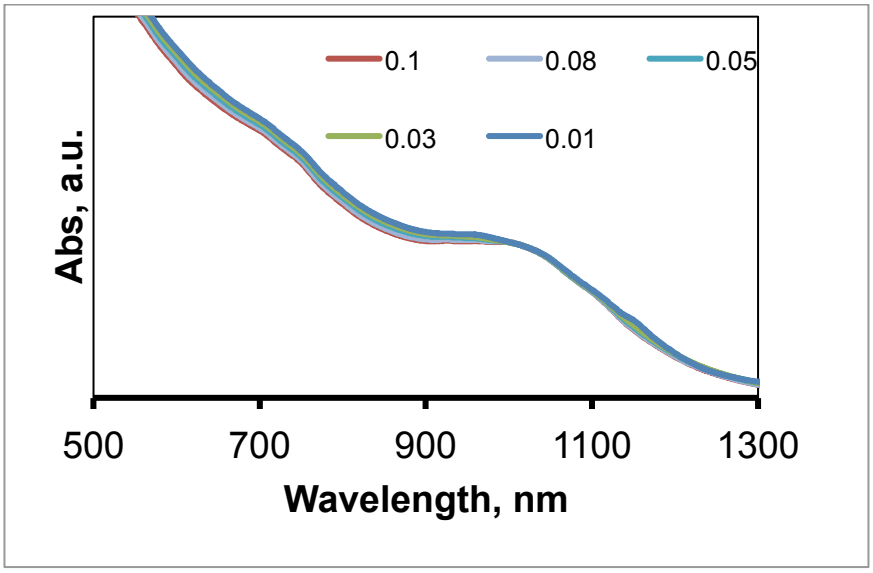

(a)

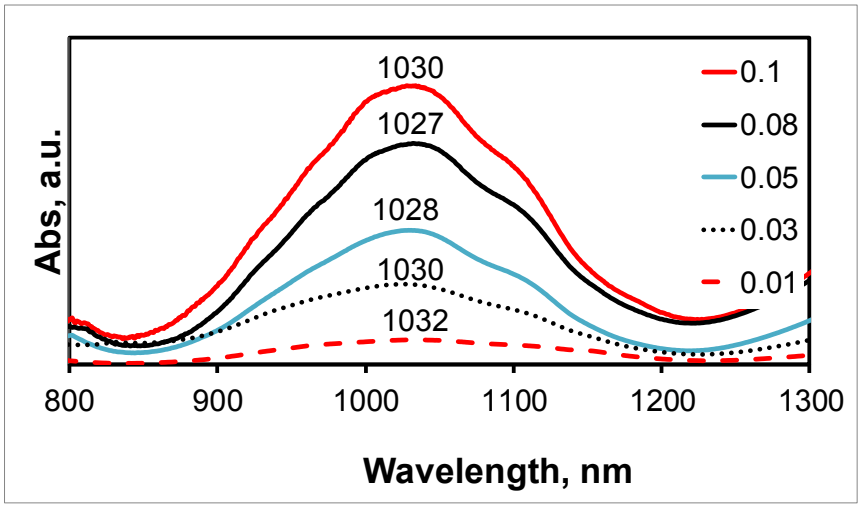

(b)

Figure 2.4. Baseline Corrections of Before Centrifugation. (a) Normalized at 1015nm (b) Linear Correction of S_{22}.

A close analysis of the purified suspensions provided insight into the effect of the starting concentration on the quality of suspensions produced. The linear correction applied slope correction for background effects using two X values. Thus, each of 0.1 mg/mL and 0.01 mg/mL centrifugal cycles were analyzed for any significant shifting in the S_{22} transition peak. In Figure 2.5a, the peak at 1015 nm was normalized for comparison since differences between the cycles of each suspension can be seen. Once again, the resolved transitional peaks were more noticeable after centrifugation. Figure 2.5b and c, 0.1 and 0.01 mg/mL respectively showed the shifting between cycles. Even though there was not a clear shifting trend with each suspension or a shifting trend with each cycle, shifting occurs with each suspension between its non-centrifugal sample and any of its centrifugal samples regardless the number of centrifugal cycles. Thus, the increased resolution of the peaks indicated that the centrifugation has separated the impurities from the suspension.

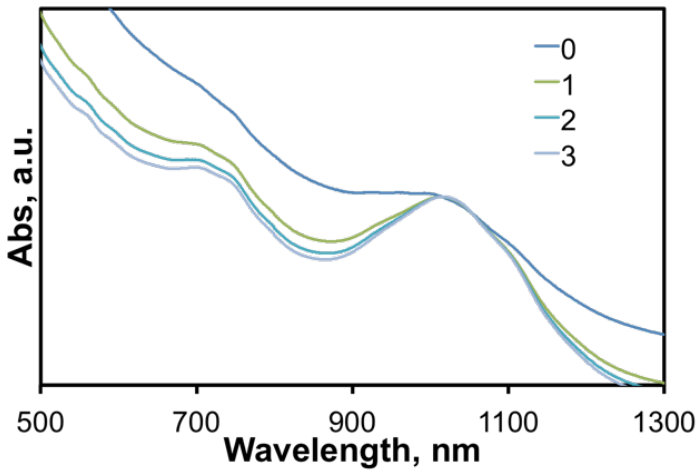

(a)

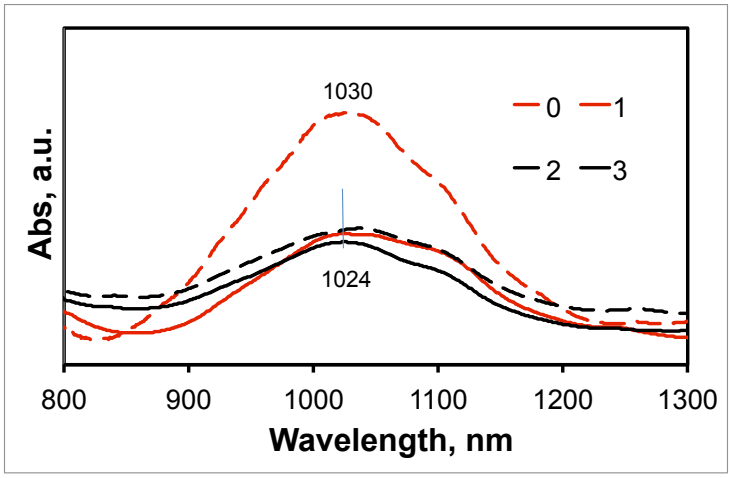

(b)

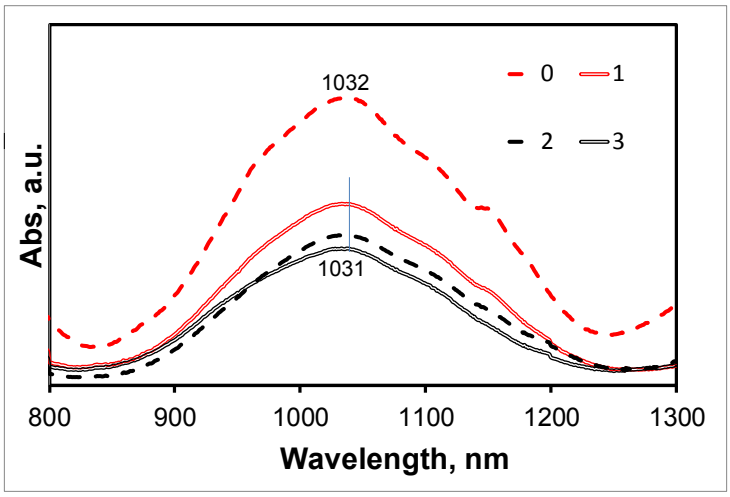

(c)

Figure 2.5. UV-vis Spectra of SWNT Suspensions. (a) 0.1mg/mL offset at 1015nm (b) Linearly corrected of 0.1mg/mL cycles (c) Linearly corrected of 0.01mg/mL cycles.

Table 2.1 reports the mean and standard deviation to have a better understanding of the peak and total area of 830-1240 nm, which are the S_{22} and S_{11} transition peaks. Using six trials, increasing ratios were observed as the number of cycle increases for each suspension. Also, as the concentration decreased, the increments in the area ratio decreased, too. Hence, the non-centrifuge sample of each suspension had a relatively similar ratio; however, the change decreased as the initial concentration decreased as well as the change between each cycle of a suspension decreased as number of cycles

increased. This confirmed that low-G centrifugation purified the suspensions by the removal of impurities. Thus, the better resolution of the peaks demonstrated that the centrifugation, again, separated the impurities from the suspension. Moreover, the small peak shift did not affect the diversity of nanotube suspension.

Table 2.1. Peak and Total Area Ratios between 830-1240nm

Conc-Cycle, PA/TA	0 C	1 C	3 C
0.1 mg/mL	0.050 ± 0.004	0.14 ± 0.02	0.17 ± 0.02
0.08 mg/mL	0.050 ± 0.002	0.140 ± 0.009	0.16 ± 0.01
0.05 mg/mL	0.048 ± 0.002	0.13 ± 0.01	0.15 ± 0.01

Raman spectroscopy characterization

Raman spectroscopy was used to study SWNTs because of its sensitivity to the symmetric covalent bonds. The spectra would inform about the vibrational and other modes in the system. Thus, the Raman bands of the sp^2 bonds can be used to show the disorder of the nanotubes. The G-band, which represented a symmetrical graphene lattice, was observed around 1590 cm^{-1}; and the D-band, which represented a disorder graphene lattice due to defects in the sp^2 bonds in the system, was observed around 1330 cm^{-1} (Figure 2.6).

(a)

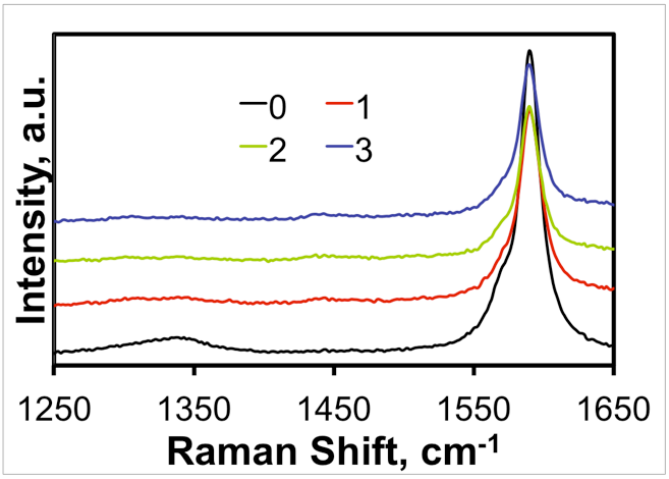

(b)

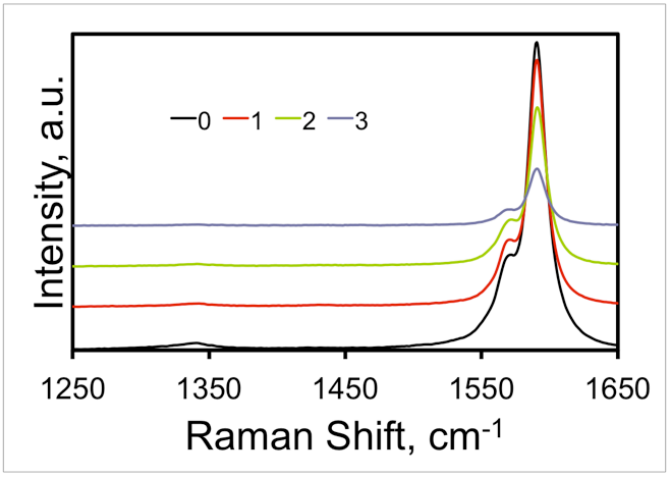

Figure 2.6. Raman Spectra of SWNTs. (a) Raman Spectra of Centrifugal Cycles of a Suspension (b) Raman Spectra of Centrifugal Cycles of a Suspension Deposited on Si wafer.

In Raman spectroscopy, bands indicated the ability of low-G centrifugation to limit such defects after each centrifugal cycle of SWNTs suspensions and to show the increase of individual SWNTs due to dispersion. Raman spectra of centrifugal cycles of a suspension were normalized at the D-band (Figure 2.6a). G-band was approximately 1590 cm^{-1}, and D-band ranged from 1300 -1340 cm^{-1}. As the amount of centrifugal cycles increased, the G and D-band intensities decreased. After the third cycle, the D

band is close to the baseline. In Figure 2.6b, observation of the SWNTs on Si surface determined a larger shoulder from the G-band than for the suspensions. Also, like the Raman spectra for the suspensions, the D-band intensity declined with more centrifugal cycles. The correlation between the band peak-to-peak intensities of SWNTs suspensions and their centrifugal cycles had previously been reported.[7] Thus in Table 2.2, the G-to-D-band peak ratios were used to show the decline trend of aggregation as well as the effectiveness of the low-G centrifugation to not damage the tubes. In addition, band intensities from SWNT suspensions instead of SWNT deposition on a substrate were chosen because of higher consistency than surface deposition.[25] Unfortunately, the average and standard deviation on some of the suspension cycles were similar. Hence, some of the variables may have not been controlled consistently. Finding the peak-to-peak ratios of SWNTs networks was done to investigate further the inconsistency of aqueous suspensions. Yet, similar to the results of the SWNT suspension, the I_D/I_G peak ratios of the networks increased after the 1C and then were inconsistent for the others.

Table 2.2. G-to-D Ratios for the SWNT Suspensions Deposited on a Si Wafer Before Centrifugation (0C), after First Centrifugal Cycle (1C), and after Third Centrifugal Cycle (3C)

Conc-Cycle, I_G/I_D	0 C	1 C	3 C
0.1 mg/mL	50 ± 20	60 ± 10	67 ± 4
0.08 mg/mL	35 ± 8	60 ± 20	40 ± 7
0.05 mg/mL	40 ± 20	50 ± 20	65 ± 25

AFM characterization

Atomic force microscopy (AFM) is a type of microscopy that can form high-resolution images of surfaces. A part of a larger branch scanning probe microscopy, AFM measures the motion of a cantilever beam with a very small mass. The force required to move this beam through measurable distances (10^{-4} Å) can be as small as 10^{-18} N. This level of sensitivity can clearly obtain resolution that is on the nanometer scale, more than the optical diffraction limit. Hence, the lateral resolution of AFM can be approximately 30 Å, and the vertical resolution can be up to 0.1 nm. Fundamentally, AFM images of the SWNT networks were produced by a sharp probe on the bottom end of the cantilever was brought close to the sample surface. The forces between the tip and the sample caused a deflection of the cantilever. That deflection was measured by a laser beam that was aimed at the top surface of the cantilever. Then, the cantilever beam reflects the laser beam from the cantilever to a position-sensitive photodetector that comprise four segments. The differences between signals generated from these segments indicated the position of the laser on the detector and thus, angular deflection of the cantilever.

Generally, AFM can be operated in three imaging modes, contact, intermittent, and non-contact. Yet, intermittent mode was used since these experiments were performed in ambient conditions, and topography of the SWNTs was desired with minimal amounts of noise and drift from the probe tip. To produce an image in this mode, the cantilever was driven to oscillate near its resonance frequency by a small piezoelectric element located in the AFM tip holder. The electronic servo controlled the height of the cantilever as it engaged the nanotube networks; therefore the damages from intermittent contacts of the tip and the sample were reduced. Finally, the force of the

contact was measured to create an image of the surface. One key advantage of this technique was that three-dimensional image was formed. Consequentially, once an image was fabricated, characteristics such as SWNT density, SWNT length, and surface height were possible to measure. For this paper, the AFM is another method to characterize the physical properties of SWNT deposited on Si surface. This was important to distinguish differences between concentrations. In addition, the impurities deposited on the surface may vary with the initial SWNT concentration.

Below are AFM images of the 0.1 mg/mL (Figure 2.7). The images were produced by placing the AFM tip in the middle of each deposited SWNT suspension. Since the AFM cantilever can scan up to 40-μm x 40-μm area, five-8 μm x 8 μm images were selected in various places. Images of different centrifugal cycles of initial concentration of 0.1 mg/mL were selected since this concentration showed more tubes and impurities and as a result, the largest change in the impurity reduction after each cycle (Figure 2.7). Before centrifugation, there were noticeable impurities represented as the white irregular shaped globules and SWNTs represented as the white lines in the image (Figure 2.7a). The height histogram inset showed the majority of the surface height approximately 10 nm, which was far above the average SWNT height of 1.2 nm. Thus, there was a necessity for centrifugation in order to reduce the amount of impurities. However, after the first cycle, the globules have decreased in size and amount. There was also a shift in the height profile towards 5 nm. Thus, even one centrifugal cycle was enough to reduce the height by half and the bigger globular impurities have been removed. Moreover, the amount of SWNTs seemed to have increased with more individual tubes being distributed evenly (Figure 2.7b). Finally, the third cycle revealed

smaller impurities compared to the first cycle. However, the amount of the impurities and SWNTs seemed to be similar. The height profile inset shows that the surface height has been further reduced to approximately 4 nm, for an overall 60 % reduction from the 0C or before centrifugation (Figure 2.7c).

(a)

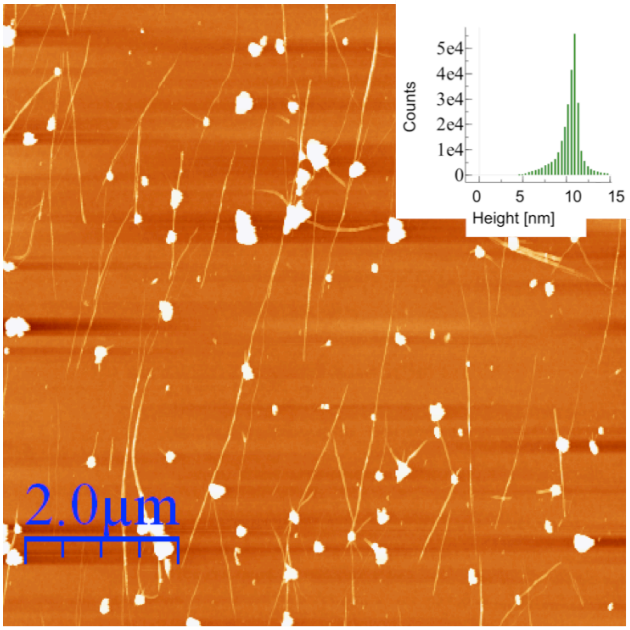

(b)

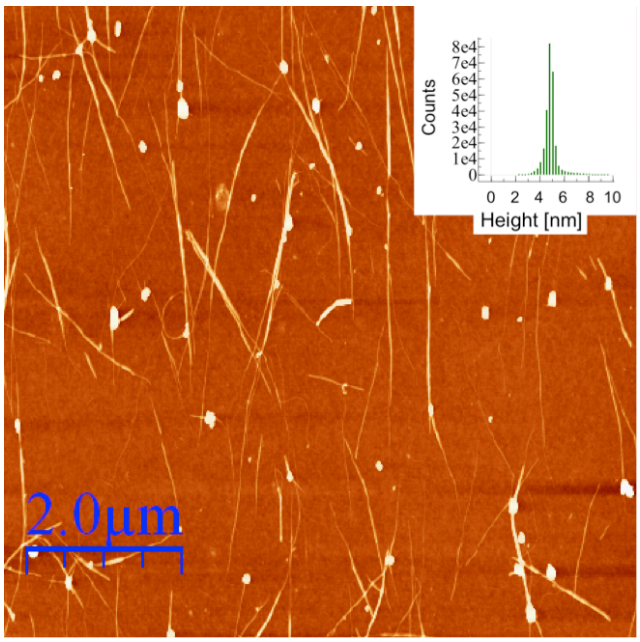

(c) 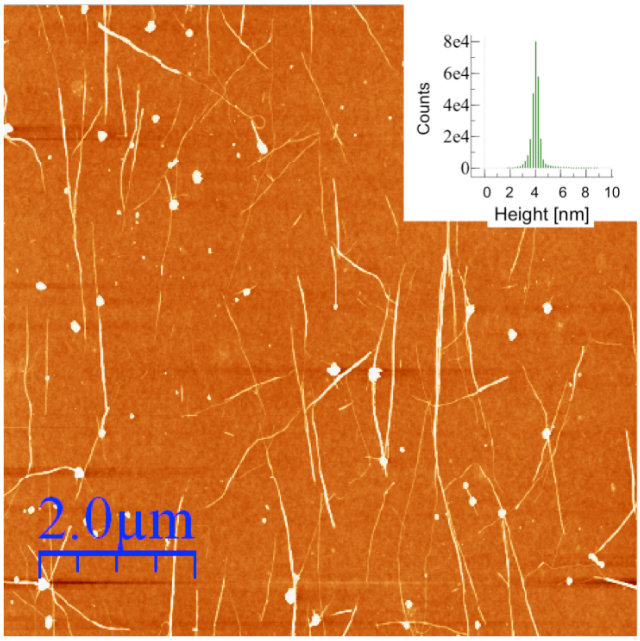

Figure 2.7. AFM Images of SWNT Deposits of 0.1 mg/mL Suspension. (a) Formed before centrifugation (0C). (b) After first centrifugal cycle (1C). (c) After third centrifugal cycle (3C). The occurrence and size of globular impurities increased with concentration, demonstrated the need purification for every concentration of SWNT soot used to form each suspension. AFM images of deposits formed after three centrifugation cycles were used to purify the SWNT suspensions showed that the frequency and average height of impurities was greatly reduced for all concentrations.

To characterize the SWNTs in each cycle of a concentration, the SWNT density, SWNT length, and surface height were determined. Table 2.3 lists the SWNT density of initial concentration, first, and third cycles for 0.1, 0.08, and 0.05 mg/mL. The density was determined by counting the number of whole SWNTs in the scanning image (8 µm x 8 µm). This determined any changes of SWNTs deposited as a function of concentration. All initial concentrations had similar amounts of tubes. Therefore, the amount of suspension deposited on the Si wafer was saturated for all concentrations and proved that

the deposition method was an ideal choice. With the exception of 0.05 mg/mL, the tube density of first and third cycles increased and then decreased. Since precision decreased for every concentration as the cycles increased, this may indicate a preference on where the SWNTs deposited. Thus, the deposition was sensitive to LFD.

Table 2.3. SWNT Density of Before Centrifugation (0C), After First Centrifugal Cycle (1C), and After Third Centrifugal Cycle (3C).

Conc-Cycle, tube# /μm^2	0 C	1 C	3 C
0.1 mg/mL	18 ± 2	32 ± 5	24 ± 5
0.08 mg/mL	20 ± 6	30 ± 4	17 ± 4
0.05 mg/mL	18 ± 4	17 ± 2	30 ± 10

Next, the average surface height generated height measurements of SWNTs and impurities. As explained in the histograms for Figure 2.7, a visual representation of the centrifugal cycle versus surface height gave insight in how centrifugation was affecting the suspensions. Table 2.4 quantifies surface heights to confirm the reduction was caused by the centrifugation. There was at least a 30 % drop from the initial concentration to the first cycle, and further decrease in the height as the number of cycle increased.

Table 2.4. Average Surface Height of Before Centrifugation (0C), After First Centrifugal Cycle (1C), and After Third Centrifugal Cycle (3C)

Conc-Cycle, nm	0 C	1 C	3 C
0.1 mg/mL	10 ± 3	7 ± 3	4.3 ± 0.7
0.08 mg/mL	8 ± 2	4.5 ± 0.7	3.1 ± 0.9
0.05 mg/mL	7 ± 3	2.7 ± 0.5	2.0 ± 0.8

Finally, SWNT length measurements were taken from SWNT counted as part of the density (Table 2.5). The 0.1 and 0.08 mg/mL samples generally stayed consistent after centrifugation unlike 0.05 mg/mL samples. The tube length became shorter as the number of cycles increased. Yet, 0.1 mg/mL had the longest tubes than any other. Furthermore, though centrifugation removed impurities, it may initially have increased the number of tubes deposited without a drastic change to the SWNT length for the two higher concentrations. Yet the 0.05-mg/mL samples may have increased their SWNT density with shorter tubes.

Table 2.5. Average SWNT Length of Before Centrifugation (0C), After First Centrifugal Cycle (1C), and After Third Centrifugal Cycle (3C)

Conc-Cycle, µm	0 C	1 C	3 C
0.1 mg/mL	1.4 ± 0.2	1.7 ± 0.1	1.7 ± 0.2
0.08 mg/mL	1.4 ± 0.2	1.3 ± 0.2	1.4 ± 0.1
0.05 mg/mL	1.5 ± 0.1	1.3 ± 0.3	1.1 ± 0.2

2.5 Conclusion In conclusion, low-G centrifugation is a method that separates SWNTs from impurities because the transition peaks become more resolved with every centrifugal cycle. This method demonstrates its degree of separation for each concentration. In the UV-vis range, the peak at 275 nm is noted visible after the first centrifugal cycle. Moreover, the resolution increases when comparing the degrees of separation of impurities between sequential cycles. Observing the interband transitions at the NIR region, all concentration had similar absorbance. Subtracting the plasmon region, the interband S_{22} peak was similar to all, and therefore, the fractions of SWNTs and impurities were the same to all concentration. Further analysis, the ratio between the

peak area and total area proves that peaks were more resolved as the cycles increased. Also, the starting concentrations have similar amounts of SWNTs and impurities. There was no shifting for different concentration as well as different cycles per suspension. For Raman, efforts should be focused on the problems that prevented the analysis of the defects or damages of nanotubes. Results showed an increase in the peak ratio of I_G/I_D bands from the initial concentration to the first centrifugal cycle for all suspensions. Hence, each concentration has SWNTs with lower structural damage available after the first cycle. Yet, peak ratios after second and third cycles were inconclusive. Thus, the study needed to be investigated further in order to characterize further the effects of low-G centrifugation on SWNTs. Finally, topographic images from AFM provided information about the density, surface height, and SWNT length. Size of globules and surface height decreased as from the 0C state to the 1C. Moreover, there was a small change in height from the 1C to 3C even though it was less than the change from 0C to 1C and topographic images of 1C and 3C appeared identical. Also, a 60 % height reduction and an increase of SWNT density after 3C were reported. In conclusion, different SWNT concentrations produce similar characteristics at 0C and after 1C only. More centrifugal cycles and less concentrated SWNT suspensions caused more fluctuations when determining characteristics for each concentration. The higher concentrations tend to have higher SWNT density and better accuracy. Thus, they are more reproducible and reliable for future SWNT-based applications.

2.6 References

1. Lee, C. W.; Weng, C. H.; Wei, L.; Chen, Y.; Chan-Park, M. B.; Tsai, C. H.; Leou, K. C.; Poa, C. H. P.; Wang, J. L.; Li, L. J. *J. Phys. Chem. C* **2008,** 112, (32), 12089-12091.

2. Nirmalraj, P. N.; Lyons, P. E.; De, S.; Coleman, J. N.; Boland, J. J. *Nano letters* **2009,** 9, (11), 3890-3895.

3. Tabakman, S. M.; Welsher, K.; Hong, G.; Dai, H. *J. Phys. Chem. C* **2010,** 114, (46), 19569-19575.

4. Vichchulada, P.; Shim, J.; Lay, M. D. *The Journal of Physical Chemistry C* **2008,** 112, (49), 19186-19192.

5. Aitchison, T. J.; Ginic-Markovic, M.; Matisons, J. G.; Simon, G. P.; Fredericks, P. M. *The Journal of Physical Chemistry C* **2007,** 111, (6), 2440-2446.

6. Li, X.; Zhang, L.; Wang, X.; Shimoyama, I.; Sun, X.; Seo, W.-S.; Dai, H. *Journal of the American Chemical Society* **2007,** 129, (16), 4890-4891.

7. Porro, S.; Musso, S.; Vinante, M.; Vanzetti, L.; Anderle, M.; Trotta, F.; Tagliaferro, A. *Physica E: Low-dimensional Systems and Nanostructures* **2007,** 37, (1), 58-61.

8. Romanos, G. E.; Likodimos, V.; Marques, R. R.; Steriotis, T. A.; Papageorgiou, S. K.; Faria, J. L.; Figueiredo, J. L.; Silva, A. M.; Falaras, P. *The Journal of Physical Chemistry C* **2011,** 115, (17), 8534-8546.

9. Shim, J.; Vichchulada, P.; Zhang, Q.; Lay, M. D. *The Journal of Physical Chemistry C* **2009,** 114, (1), 652-657.

10. Wang, Y.; Gao, L.; Sun, J.; Liu, Y.; Zheng, S.; Kajiura, H.; Li, Y.; Noda, K. *Chemical physics letters* **2006,** 432, (1), 205-208.

11. Svedružić, D.; Blackburn, J. L.; Tenent, R. C.; Rocha, J. D. R.; Vinzant, T. B.; Heben, M. J.; King, P. W. *Journal of the American Chemical Society* **2011,** 133, (12), 4299-4306.

12. Sarker, B. K.; Shekhar, S.; Khondaker, S. I. *ACS nano* **2011,** 5, (8), 6297-6305.

13. Asada, Y.; Miyata, Y.; Shiozawa, K.; Ohno, Y.; Kitaura, R.; Mizutani, T.; Shinohara, H. *The Journal of Physical Chemistry C* **2010,** 115, (1), 270-273.

14. Mistry, K. S.; Larsen, B. A.; Bergeson, J. D.; Barnes, T. M.; Teeter, G.; Engtrakul, C.; Blackburn, J. L. *ACS nano* **2011,** 5, (5), 3714-3723.

15. Lipscomb, L. D.; Vichchulada, P.; Bhatt, N. P.; Zhang, Q.; Lay, M. D. *Journal of Materials Science* **2011,** 46, (21), 6812-6822.

16. Yu, A.; Bekyarova, E.; Itkis, M. E.; Fakhrutdinov, D.; Webster, R.; Haddon, R. C. *Journal of the American Chemical Society* **2006,** 128, (30), 9902-9908.

17. Carvalho, E. J. F.; dos Santos, M. C. *ACS nano* **2010,** 4, (2), 765-770.

18. Kim, P.; Odom, T. W.; Huang, J.-L.; Lieber, C. M. *Physical review letters* **1999,** 82, (6), 1225.

19. Miyauchi, Y.; Oba, M.; Maruyama, S. *Physical Review B* **2006,** 74, (20), 205440.

20. Strano, M. S.; Dyke, C. A.; Usrey, M. L.; Barone, P. W.; Allen, M. J.; Shan, H.; Kittrell, C.; Hauge, R. H.; Tour, J. M.; Smalley, R. E. *Science* **2003,** 301, (5639), 1519.

21. O'connell, M. J.; Bachilo, S. M.; Huffman, C. B.; Moore, V. C.; Strano, M. S.; Haroz, E. H.; Rialon, K. L.; Boul, P. J.; Noon, W. H.; Kittrell, C. *Science* **2002,** 297, (5581), 593.

22. Zheng, M.; Jagota, A.; Strano, M. S.; Santos, A. P.; Barone, P.; Chou, S. G.; Diner, B. A.; Dresselhaus, M. S.; Mclean, R. S.; Onoa, G. B. *Science* **2003,** 302, (5650), 1545.

23. Rance, G. A.; Marsh, D. H.; Nicholas, R. J.; Khlobystov, A. N. *Chemical Physics Letters* **2010,** 493, (1), 19-23.

24. Vichchulada, P.; Cauble, M. A.; Abdi, E. A.; Obi, E. I.; Zhang, Q.; Lay, M. D. *The Journal of Physical Chemistry C* **2010,** 114, (29), 12490-12495.

25. Jacobsen, N. S.; Pantano, P. *Carbon* **2011,** 49, (6), 1998-2006.

26. Itkis, M. E.; Perea, D. E.; Jung, R.; Niyogi, S.; Haddon, R. C. *Journal of the American Chemical Society* **2005,** 127, (10), 3439-3448.

CHAPTER 3

INVESTIGATING COFFEE-RING DEPOSITION METHODS FOR 2-DIMENSIONAL SWNT NETWORK FORMATION[2]

[2] Stanley, D.M. and M.D. Lay. To be submitted in J. Mat. Sci.

3.1 Abstract Two evaporation-controlled, convective self-assembled methods that deposit single-walled carbon nanotube (SWNT) suspension onto a substrate as a way to control 2-dimensional (2D) SWNT networks were explored. After incubation and then dried with a stream of N_2 gas, samples were analyzed by atomic force microscopy (AFM) to determine height and roughness information. AFM images revealed that the edges contain more SWNTs than the center of the droplet. This observation was due to the "coffee-ring" effect. The influences of the ring-like structures on the volume of SWNT droplet and the incubation period were also reported as a way to control 2D formation of SWNTs. The immerse method showed evidence of high evaporation rate and more impurities as compared to the drop method. Forming small SWNT networks randomly have few inter-network connections. Therefore, the evaporation rate limited the SWNT patterns. In addition, the large drop area limited the network formation. However, the drop method had various drop areas that were smaller than constant area of droplet of the immerse method. Subsequently, there were fewer impurities, and the evaporation rate was reduced. Thus, lower volumes and times were used to study 2D patterns and network formations. An increased 2D patterns and networks were seen. Furthermore, the drop method formed dense SWNT networks; volume can control evaporation rate and repeatability; and evaporation time can control 2D patterns over 3D patterns and impurities.

3.2 Introduction Single-walled carbon nanotubes (SWNTs) have electrical properties that have been explored based on individual nanotubes to create SWNT-based devices. Yet, this route has proven unviable since the subsequent materials produce a low current, are irreproducible, and/or presented an enormous challenge for wide-scale fabrication.[1,2]

SWNT networks offer advantages over individual nanotube-based devices since they can create complex hierarchical structures easily via liquid deposition methods. Thus, creating thin films of SWNT networks is the optimal route to take advantage of its properties without difficulties of depositing a single tube onto a substrate.

Finding procedures to form SWNT devices that are reproducible and tunable directs toward the formation of 2-dimensional (2D) SWNT networks. Since high SWNT density or bundled SWNTs such as 3-dimensional (3D) networks will produce metallic conductivity, the SWNT density determines the electrical properties of SWNTs. Devices that exhibit semiconducting properties need a low density of unbundled SWNTs with high-aspect ratios. Additionally, these networks can be tuned to any degree of semiconducting behavior based on the number of SWNTs in the network. Yet, assembly of low-density networks requires the control over direction at a certain location. Thus, creating a technique that allows 2D SWNT network formation and the ability to manipulate the alignment is highly desirable.

Several studies have integrated evaporation as a part of a deposition method since it exploits a simple way to yield highly ordered structures for nonvolatile solutes.[3-8] For example, Dimitrov and Nagayama found that array formation dried in one direction is manipulated by particle diameter, its concentration, and receding rate of the film-meniscus contact line. They derived an equation that predicted growth of these arrays.[3] In our group, different controlled-evaporative techniques were studied to control the SWNT density. Here, each technique produced SWNT networks that were 2D, 3D, or combination of both and have tunable conductivities.[8] Thus, evaporation of SWNT suspensions combined with a drying process serves a great possibility for the formation

of low-density, 2D SWNT networks. In addition, ring-like deposits along the perimeter of the droplet due to "coffee-ring" effect can be used to achieve the spatial arrangements with these deposits. This phenomenon is commonly seen in drops with dispersed solutes.[9-11] As for the SWNT droplets, unbundled, high-aspect ratio SWNTs may form 2D networks by flowing away from contact line or bonding to the substrate before moving towards the droplet periphery, which will result in a uniform deposit. Hence, depositing methods driven by evaporation can control the type of SWNT network formation. Our group reported the creation of these thin films of SWNT networks that are 2D and have tunable electrical properties, using controlled evaporative methods.

Developing a feasible depositing method that utilized the evaporation process coupled with convective assembly on sessile SWNT droplets to drive 2D SWNT network formation and observed the effects of the coffee-ring phenomenon on the 2D formation was the focus of this study. Two approaches were developed and then, evaluated with a broad range of different volumes and times. The effectiveness of these methods was characterized by AFM. The hypothesis created was that the 2D SWNT networks were the function of time with respect to volume and not just time; also surface area of the droplet (size of droplet or average thickness of the droplet) may play an important role in these formations.

3.3 Experimental Methods

SWNT suspension preparation

To form suspensions of unbundled SWNTs with high-aspect ratios, a probe sonication (Branson, 250) was used to disperse as-produced, arc-discharge SWNTs (Carbon Solution Inc.) in 1% sodium dodecyl sulfate solution while minimizing damage

for 30 min at 12 W. Next, a low-G centrifugation process was repeated for 45 min at 18,000 G (Beckman, GS-15R) where top half of supernatant was decanted after each cycle. Afterwards, purity of these stable suspensions, verified with UV-VIS-NIR spectroscopy (Varian Cary 5000) and Raman microscopy (Thermo Fisher, DXR), was composed of 0.03 mg/mL SWNTs for depositing the networks.

Substrate preparation

Silicon wafers were cleaned with CO_2 before deposition of 10 mM (3-aminopropyl) triethoxysilane (APTES, Aldrich) in ethanol for 45 min. After incubation, water and ethanol rinsed the silane solution off the wafer and then dried with N_2 gas. Finally, CO_2 removed excess layers of APTES to yield a monolayer.

SWNT network formation

Two methods were performed to compare their efficiency to control the density of SWNT networks. The morphology of subsequent SWNT networks from each method was examined with intermittent mode atomic force microscopy (AFM, Pico Plus, Molecular Image). Average height from the height histograms was generated from image analysis software (WSxM v 5.3).[12] Both methods were performed under a humidity range of 27—51 % and temperature range of 74—80 °F. For the immerse method, the suspension was distributed the entire 1 x 2 cm substrate at varies volumes 50, 60, 70, 80, 100, 200, and 300 μL (Figure 3.1a). With a constant area and a known volume, an average height was determined. After an incubation time, the suspension was dried with a stream of N_2 gas, rinsed with nanopure water to remove the surfactant, and then dried again with N_2 gas. Based on the gas flow that dried the surface, five images from the center, top, sides, and bottom of the wafer were obtained (Figure 3.1b).

For the drop method, a drop of the SWNT suspension was incubated on the substrate for a certain time. Experiments were performed under a humidity range of 27—51 %, having a median of 41 %, and temperature range of 70—80 °F, having a median of 74.4—74.7 °F. Seven volumes were chosen to compare their efficiency to control the density of SWNT networks. The volumes were 1, 5, 10, 20, 30, 40, and 50 µL. For the deposition method, droplets of the SWNT suspension were incubated on the substrate for three different times of 1, 3, and 5 minutes. AFM was used to raster-scan five images on the top, sides, and bottom of the edge as well as the center of the droplet (Figure 3.2). Then, more images were produced to assess closely the edges of the droplet. Five images from inner, middle, and outer of each area of the edge were obtained (Figure 3.3).

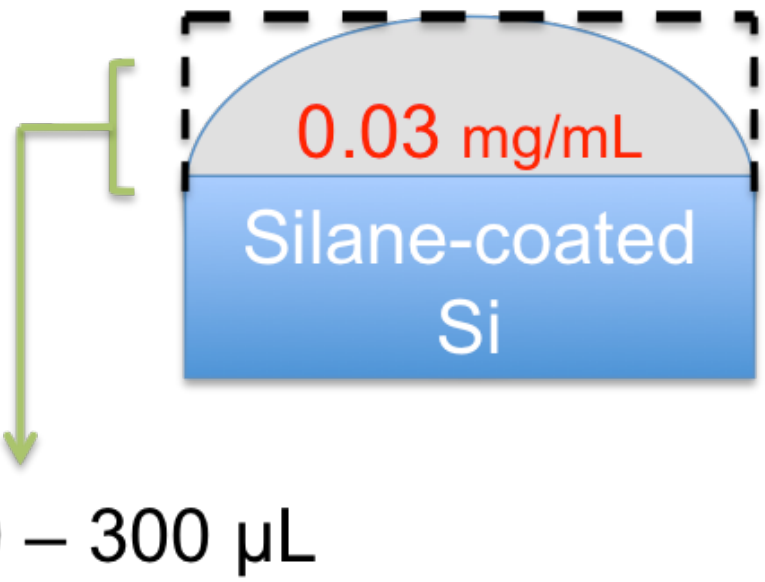

(a)

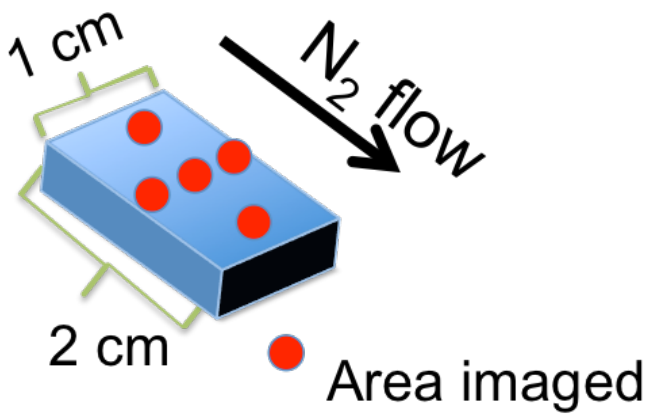

(b)

Figure 3.1. Schematic diagram of the immerse method. (a) The solution covering the entire silane-coated Si/SiO_x fragment. Droplet covered the entire surface at given volumes to yield average thicknesses. (b) The size, direction flow of N_2, and images that were taken as indicated by the red dots of the fragment.

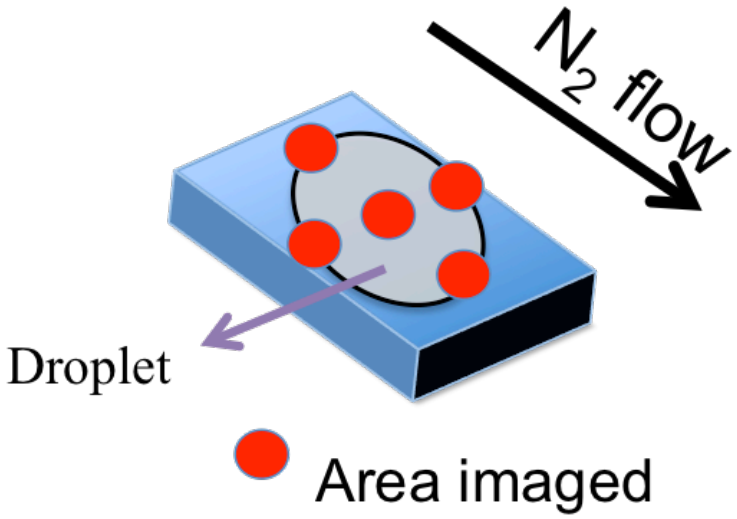

Figure 3.2. Schematic diagram of the parameters of drop method for preparation and data collection. A droplet was placed on silane-coated Si/SiO_x wafer. The direction flow of N_2 that dried the droplet and images that were taken as indicated by the red dots of the fragment are shown.

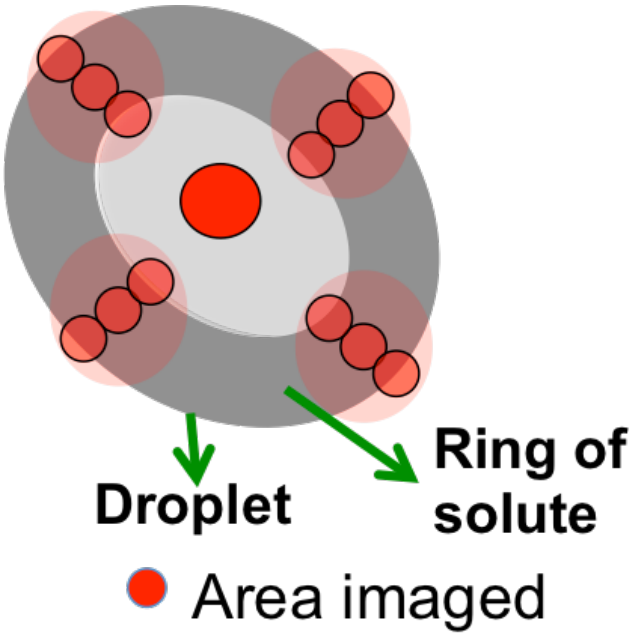

Figure 3.3. Schematic diagram of a closer view of the coffee-ring for the data collection of the drop method. A droplet was placed on silane-coated Si/SiO_x wafer, dried with N_2 gas, and images that were taken as indicated by the red dots of the fragment are shown above. Image of the droplet's edge is enlarged to show the sets of images taken at the outer, middle, and inner parts of the edge as well as the center of the droplet.

3.4 Results and Discussion

Immerse method—Constant droplet area

Since the pinning of the contact line drives the coffee-ring (CR) effect, the initial emphasis was to understand how surface area affected 2D network formation in the droplet. Observing different volumes and evaporation times aided in this study. Hence, the area of the droplet was held constant for the first method. The SWNT suspension covered over the entire substrate induced a convection driven by surface tension in the droplet. Thus, this effect may lead to an even and well-controlled drying process. Since

the droplet formed a hemisphere, an average height of the droplet can be obtained as a way to correlate surface area of the droplet with the evaporation process.

Seven volumes were chosen (50, 60, 70, 80, 100, 200, and 300 µL) for the volumetric study, based on the average height of the droplet. This revealed that volume could predict 2D formations. As the result, average height of the surface showed a general decline, as the volume increased (Figure 3.4). The volumes of 50, 60, and 70 µL showed evaporation started on the corners of the substrate, probably due the volume used at the corners was the lowest when compared to the edges and center of the droplet. 50-µL samples have the largest degree of evaporation. Then, 60 and 70 µL have significantly less percentage of evaporation. Images from these volumes were highly packed with 3D SWNT bundles. This was confirmed by the decreasing average surface heights respectively. For the higher volumes, there was a noticeable difference of the number of SWNTs towards the edges than the center, which confirmed the CR effect.

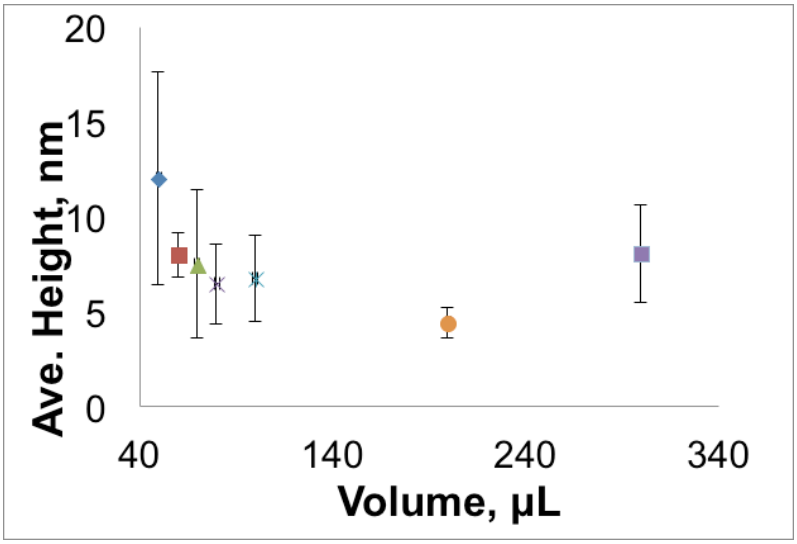

Figure 3.4. Volumetric Study at 10 min for 50, 60, 70, 80, 100, 200, and 300 µL. Large variance for the lower volume was due to evaporation. The average height stabilized as the volume increased. However, there was a difference in patterns and SWNT density.

Another observation was the large variance seen from the results of 50, 60, and 70 µL. This suggested that 3D patterns and impurities have deposited after the network formation process (Figure 3.5). These deviations occurred in the higher volumes even though the contact line did not recede as greatly as 50, 60, and 70 µL. The experiments were performed in ambient conditions where the room temperature ranged from 74—80 ^{0}F, thus bench top where the substrate lied had been at a constant temperature. Furthermore, instabilities, particularly Marangoni effect, were not documented since there was not temperature gradients in the droplet.[10,13] These temperature gradients could have caused by the random spatial arrangements.

(a) 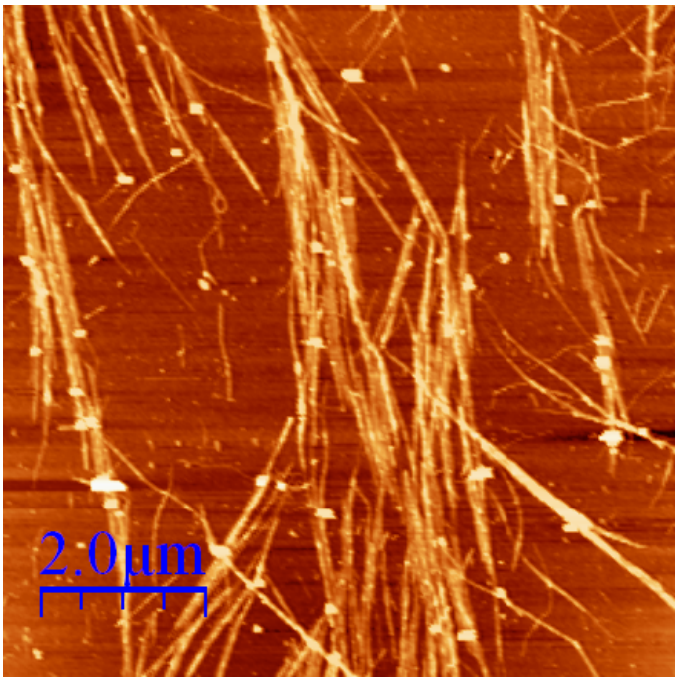

(b) 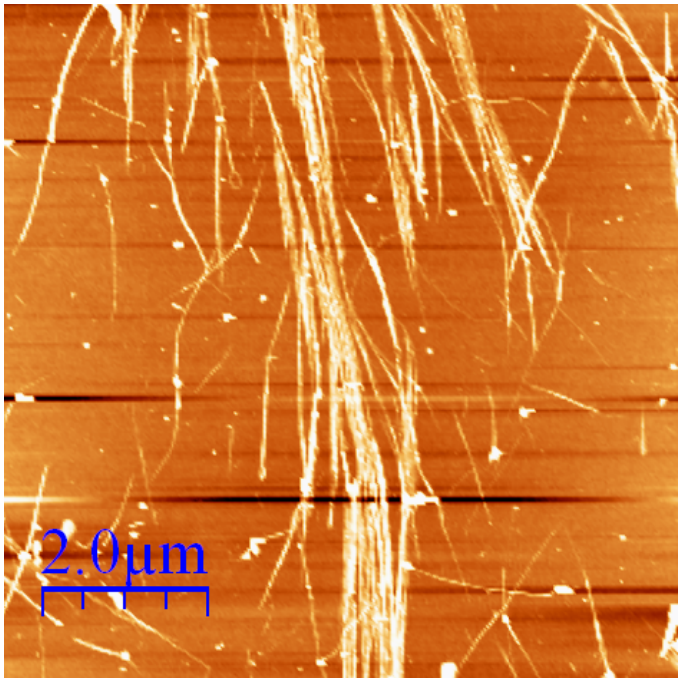

Figure 3.5. AFM image of 60 µL. (a) Right side of the substrate (b) Center of the droplet. There were noticeable amounts of impurities. The highly aligned SWNT density of the 2D networks was more abundant on the sides of the substrate than center. Yet due to evaporation, 3D networks were also abundant.

A temporal study done using 80, 100, and 200 µL also predicted the 2D networks since CR effect begin to be observed without noticeable signs of evaporation. The average height showed an upward trend like the 80-µL study. Finally, the 200-µL studies showed that the trend for average height inconclusive. Possibly since the average droplet height was around 0.1 cm, a higher temporal selection was needed to draw a conclusion about the average surface height (Figure 3.6). The lack of trend suggested that a larger percentage of the SWNTs are being removed during the drying process. Thus, a trend was seen for the 80-µL samples, instead of the 100 or 200-µL samples. Perhaps an increased incubation time was needed to ensure that the tubes are securely attached to the substrate.

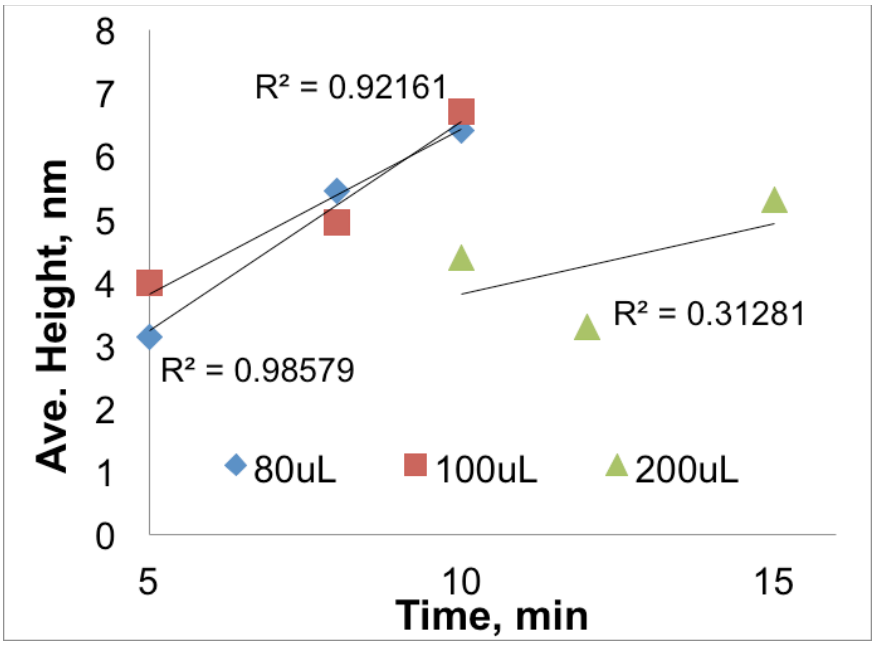

Figure 3.6. Temporal Study using 80, 100, and 200 µL. The different R^2 values suggested that SWNT patterns of 80 µL and 100 µL are more predictable than 200 µL. As the volume increased, less SWNT networks were found. Instead 1D patterns or single SWNTs were abundant.

In summary, for the volumetric studies, height increased as volume decreased; volumetric and temporal adjustments predicted the optimal parameters for 2D bundles to develop. If large degree of evaporation had occurred then, the 3D bundles were more prevalent than if there was little or no evaporation observed. The significant evaporation from the 50, 60, and 70-µL studies formed plenty of 3D and 2D networks. Evaporation at the corners of the substrate was seen for volumes of 50, 60, and 70 µL (average drop height of 0.25, 0.3, 0.35 mm respectively), which increased the amount of evaporation as the volume decreased. Temperature gradients did not caused the high variance in the average surface height for the lesser volumes.

Drop method—Various droplet areas

Since uneven patterns were discovered from the immerse method, the drop method that placed a drop without disturbance until it was dried was proposed to eliminate the high deviation for the average surface height. Again, the method was designed to control the formation of 2D bundles by varying the volume of the dispersed SWNT solution and its incubation time on the substrate. Additionally, the effects of the CR structures on the 2D formation and the droplet surface area were observed. This differed from the first method since its focus was discerning the effect of droplet surface area based on volume and time only.

Each volumetric trial required a new sample, and each temporal trial required three different samples. To determine the accuracy of the height and roughness measurement, the area of each droplet sample was calculated. Since the area of the droplet influences evaporation rate, any variations of the area between samples fluctuated the height measurements. Thus, a trend cannot be established, and the measurements were not accurate. Moreover, comparison of the droplet areas established the ideal volume to perform this method using different vinyl silanes. Hence, an accurate study can determine the effectiveness of the deposition method to other self-assembly monolayers.

The areas of samples with lower volumes from 1 to 30 μL were relatively close. Meanwhile the areas of samples from 40 and 50 μL trials had noticeable different between the temporal trials. Deciding which volume to use for further studies required observing the consistency of the deposition as well as the quantitative data. The 20-μL and 30-μL temporal trials both were consistent in depositing the solution onto the wafer

compare to the other lower volumes. However, the 20-µL trials showed more evidence of 3D bundles on the AFM images and histograms. The 30-µL trials have more 2D bundles than 3D bundles as well as more depositing consistency than 20-µL. Thus, the volume 30 µL can be used as the standard for further studies on 2D formation using the CR effect (Figure 3.7).

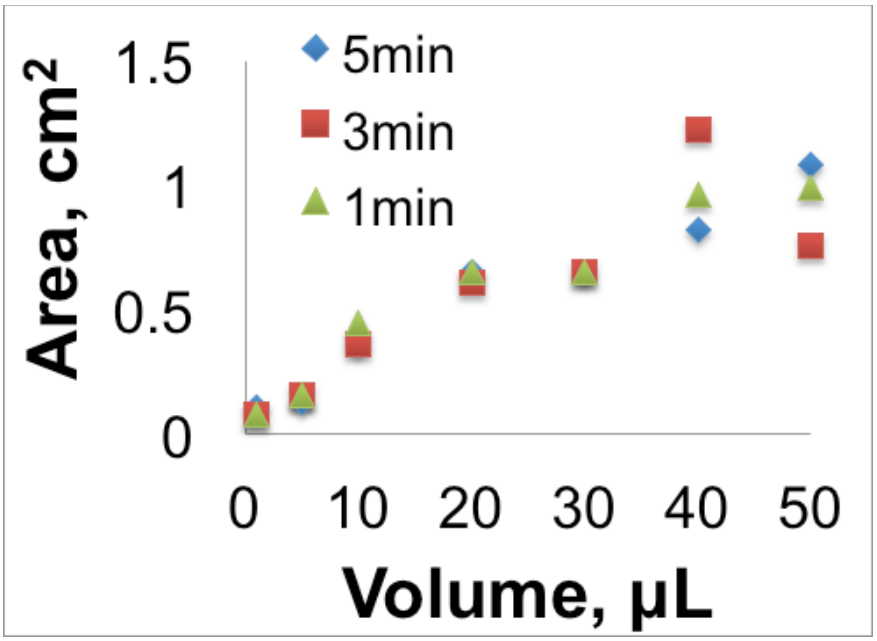

Figure 3.7. Area of each sample for each volume. Trials of 30 and 20 µL consistently spread very similar area. Height and roughness were less affected by evaporation rate; thus, results were more reliable than the other volumes.

Based on these preliminary results, a hypothesis was postulated that 2D SWNT network formation could be obtained at any volume and any time. To prove this hypothesis, more images of the edges were obtained (Figure 3.3). The first volume examined was 50 µL at 1, 3, and 5-minute trials (Figure 3.7). The average surface height at the edges of the droplet was overall higher than the center. Other volumes (1, 5, 10, 20,

30, and 40 µL) were performed at the same time trial in order to further investigate morphology of the ring-like structure.

Drop method: Height as a function of volume at constant time

When time was held constant, the volumetric trends were evaluated by recording the average height of the peripheral ring of the droplet. The general height trend suggested how the volume influenced it (Figure 3.8). The height of 1 and 3 min were the same for the 10 µL. For 20-µL studies, there were slight increases in height where the height at 3 min for the 20-µL sample was at the highest value. There was a steady downward trend for the height as the volume increased, as expected. At 3 min, the height result was higher than at 5 min, except 30 and 10-µL samples. In addition, the 10-µL sample had the highest height for the 5 min.

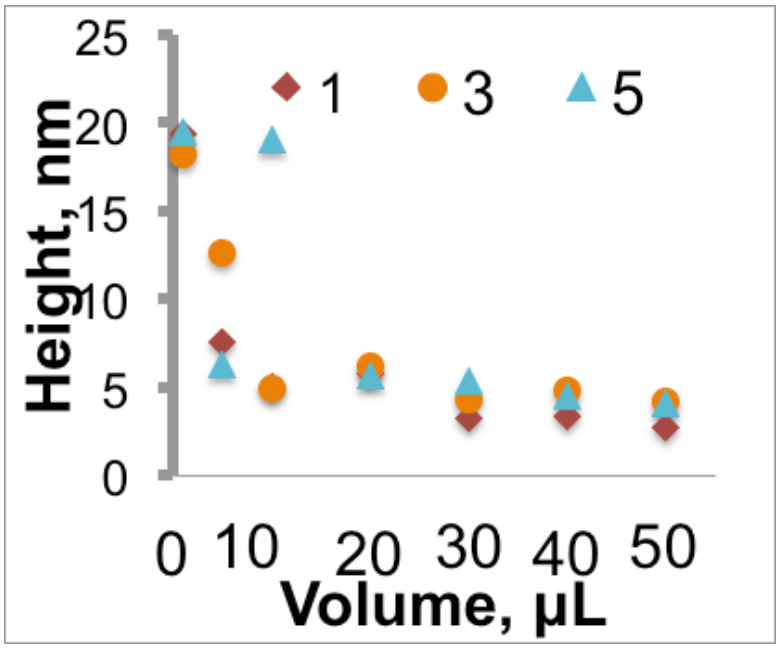

Figure 3.8. Height averages of all border of the droplet at constant time. Except for the 10-µL sample at 5 min, there was a general downward trend as the volume increased.

The results for 1-μL samples differed dramatically, in comparison to the others. Results were seen from 4 to 10 nm in height and 1 to 4 in roughness.

Examining the border of the droplet at each time was analyzed further. Looking at height at 1 min, the 10 and 20 μL increased in the height, whereas the 20 μL had the highest results. The rest of the volumes fall between 3 and 4 nm. At 3 min, as 10 and 20 μL increased in height for the outer layer, similarly to the results at 1 min, from 6 to 9 nm. Yet, the rest fall between 4 and 5 nm. Analyzing the results at 5 min, the outer layer of 10 μL drastically increased height and RMS roughness, estimated at 50 nm and 14. The height for the rest was between 4 and 8 nm. The outer layer had more changes to occur as time increased and volume decreased. The middle and inner layers of each volume have a small range of change between ± 4 nm.

Finally, exploring how the volume affected the different location of the droplet, the droplet was divided into sections that correspond to the direction of the N_2 gas. Thus, the top section was where the origin of the gas flow, and the bottom was the end of the gas flow. Left and right sections were decided on the direction of the N_2 flow. Height values of the outer layer fluctuated from 4 to 20 nm. The 10 and 20 μL have significantly higher values than the other volumes. Top section of 20 μL had the highest height value. The middle and inner layers have a narrower range. In other words, height equaled from 2 to 5 nm for middle layer. For inner layer, the height ranged between 2 and 4.5 nm.

For the outer layer, right section of 20 μL had the highest values. The top section had a similar height value to the right section. In the middle layer, as the volume increased, height range increased between the sections. Finally in the inner layer, the height varied by a couple of units when comparing each section at a volume. For the

outer layer, 10-μL sections have the highest values; the bottom and top have the higher height value than the left and right. Thus, there may be more organized bundles for the top and bottom sections. AFM images and histograms were used to confirm this speculation. Middle and inner layers also have similar values.

Difference was seen between the top of the droplet, where the N_2 gas streams began, and the bottom, associated with the size and the spacing the SWNT clusters. For all of the volumes, the bottom of the ring had smaller clusters and their spacing was farther apart (Figure 3.9). This may be due to the force of the N_2 stream pushing the nanotubes off the substrate. Hence, these thinner clusters have fewer junctions to connect networks. Moreover, as the result of the gas stream, another trend was seen at the bottom section of the ring. SWNTs or small clusters surrounded a large cluster, yet there were no junctions to connect the large cluster to the smaller ones or individual tubes. These trends caused problems dealing with electronic connections since the chance of electron hopping decreased (Figure 3.9b). Whereas the top of the ringlet usually showed more uniform networks that were wider and shorter than ones at the bottom of the ring. Also, there were more crosslinks with other SWNT clusters. The uniformity became more evident as the time increased and as the layer got closer to the inside (Figure 3.9a).

(a)

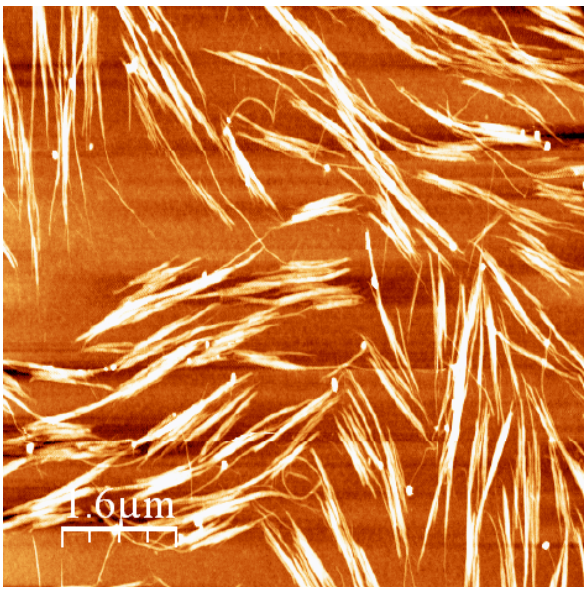

(b)

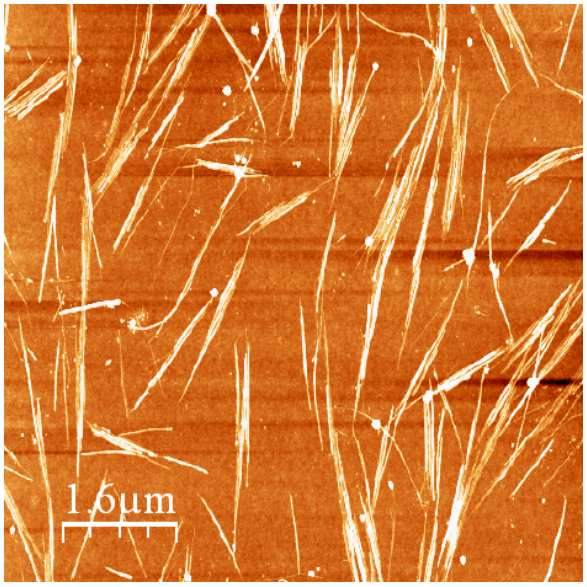

Figure 3.9. AFM images of ringlet using 40 µL and 5-min evaporation time. (a) Top of the ringlet that had more and wider networks connected to one another. (b) Bottom of the ringlet that had fewer SWNT connections and thinner 2D networks.

In conclusion, similarly to the previous method, for volumetric studies, the surface height increased as volume decreased. Volumetric adjustments can create 2D bundles formation. Yet, based on the images collected, the N_2 flow seemed to control the direction of the tube in the middle of the drop, from top, then center, and finally bottom,

more than the right or left sides of the drop. Since the droplet area varied with each volume, comparable average droplet heights can be created and hence, the lower volumes of 10, 20, 30, and 40 μL were tested. Further analysis revealed that the average cross-section height for the tubes for any volume was between from 2 to 4 nm for the top, center, and bottom; and from 3 to 5 nm for the sides after 5-min incubation. The average cross section height for the tubes after 3-min incubation was between from 1 to 3 nm for the top, center, and bottom; and from 2 to 4 nm for the sides.

Drop method: Height as a function of time at constant volume

Initially, the overall border average of the droplet at each time was examined for general trends as well as deviations (Figure 3.10). At the center of the droplet, since more evaporation occurred as the volume of the droplet decreased, there was a slight increase in the height and RMS roughness as the volume decreased. In addition, as the time increased, another slight increase was observed. The height fluctuated for 50, 40, and 20 μL. Usually a slight increase from the 1st to the 3rd min was observed, yet a decrease at the 5min. The 30-μL studies resulted in a steady increase from approximately 3 nm to 5 nm. For 10-μL studies, the height decreased at 1 and 3 min, approximately 5 to 4.8 nm, then increased drastically to 19 nm.

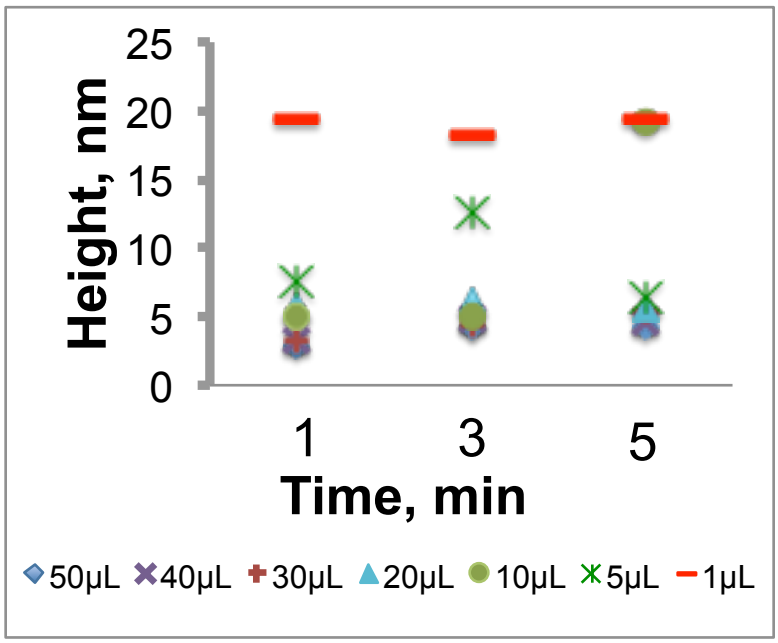

Figure 3.10. Height averages of the droplet at constant volume. Signs of evaporation were evident by the high average height for the lower volumes of 1, 5, and 10 µL for all temporal trials. However, small changes in the average height were noticed for the higher volumes.

The height averages for layers of 10-µL showed that the outer, middle, and inner layers at each time. This explained the reason for a higher standard deviation at 5 min. At the outer layer at 5 min, height increased 6-fold from other temporal trials. Analyzing the layers of 20 µL, the outer layers for each incubation time decreased as the time increased, 9.3, 8.9, and 7.5 nm respectively. The relative standard deviation increased as the time decreased. Interestingly, at 1 min, the relative standard deviation was 68 %. For the 3 and 5 min, the relative standard deviations were 40 and 44%, respectively.

For 10 µL of the outer layer section averages, the bottom section was the highest at 5 min and the lowest for 1 and 3 min. For the height at 1 min, the values increased from bottom, left, right, and top. The height increased for the left and bottom sections.

The height values were lower for the right and left sections than top and bottom. Maybe that was due to impurities or more disordered. Furthermore, the AFM images and height histograms verified that there were more impurities on the sides or more 3D bundles. For the middle and inner layers of 10 μL, bottom sections have the lowest values; however, top section and either left or right section have the highest roughness values. For 20 μL of all layers section average, the outer layer of the bottom section had the lowest values with top section having the highest height value at 1min. As for the left and right sides, usually the highest RMS roughness values was observed on either side at all times. For the middle layer, a general increase was seen with increasing incubation time, except for bottom section. The bottom section had the highest values for 1 and 3 min. Similarly to middle layer, an upward trend was seen for the inner layer. Also, the top layer had the highest roughness. For the 30 μL of all layers section averages, the outer layer showed general upward trend as the time increased. Small change in the values as the time increased. Top section for roughness was the highest; bottom section was the lowest. For the middle layer, it was the same as the outer layer, except right section for 5 min had the highest values. The inner layer had similar results as the middle layer. As for the 40 μL of all layers section averages, 1 and 3 min have a narrow range for all values. For values from 3 min to 5 min, the outer layer, values increased 3-fold. For middle layer, the height values increased 2.5-fold and 2-fold increase for inner layer. Finally, the 50 μL of all layers section averages showed that the outer layer at 3 min had the highest values than the 5 min.

Signs of evaporation were seen for the 1 μL at 3 and 5 minutes. At 5 min, the majority of the solution had evaporated and, hence the average height was very high in

comparison. At 3 min, the bottom portion of the droplet had evaporated, where the evaporation began. In addition, the average height at 1 min is over 40 nm, even though there were no observed signs of evaporation. The other areas of the droplet showed signs of evaporation. Thus, this volume would not be ideal for 2D SWNT networks.

Even after 5 min, 40 nm was measured as the average height, which was high. Interestingly, when comparing this volume to height of 10 μL was the similar. The other areas of the droplet showed signs of evaporation. Thus, this volume would not be ideal for 2D SWNT of the outer layer from the 1 and 3-minute trials, even though the other two layers showed an increase as the time increased. This behavior could be possible that SWNTs were not moving towards the scanned location. Thus, this would explain the randomness seen in the different sides on the outer layer at different times.

3.5 Conclusion This study documented the spatial-temporal evaporation of two methods, immerse and drop. Drop method was better deposition method because the number of the tubes versus impurities was higher and easier to obtain the CR. The average height of the deposited SWNTs increased as the evaporation time increased, except for the lower volumes of the immerse method. Further analysis of the drop method revealed that lower volumes have a more consistent deposited area. Other factors that were observed were the relative humidity and temperature during deposition. Even ten-point temperature range showed no signs of trends for both methods. Yet for the drop method, there seemed to be an increase of deposited particles as the relative humidity increased.

In the temporal and volumetric studies, each droplet was measured multiple times in multiple areas using AFM. In both studies, the measurements were made for three variables (average height, border layers, and the sides of droplet) from 1260 images,

excluding the 105 images in the center of the droplets. Also, the overall averages of height were not included as variables. Since average height was a measurement of impurities and SWNTs on the surface, the expectation was this variable would reflect the border layers created by CR effect and sides of the SWNT droplet. In the previous sections, the regression was considered on only two or three variables. Moreover, in both studies, the linear relationship between the average height and border layers appeared stronger than the linear relationship between the average height and sides of the droplet. Thus, the CR effect had a stronger influence on the formation of 2D bundles and SWNT density than the evaporative technique. This means that a variation on how the droplets were deposited and dried have lesser effects on the SWNT network formation.

Though that conclusion was directly established, it did not allow some questions to be investigated. These questions, for example, deal with defining the relationship between average height and border layers when the sides were adjusted or similarly, the relationship between average height and sides when the border layers were adjusted. Additionally, the previous analyses may not be able to answer important questions about the relationship observed when the temporal and volumetric studies were combined to understand how time and volume can be used to optimize 2D bundle formation and SWNT density.

3.6 References

1. Choi, S.-J.; Bennett, P.; Takei, K.; Wang, C.; Lo, C. C.; Javey, A.; Bokor, J. *ACS nano* **2012,** 7, (1), 798-803.

2. Bachtold, A.; Hadley, P.; Nakanishi, T.; Dekker, C. *Science* **2001,** 294, (5545), 1317-1320.

3. Dimitrov, A. S.; Nagayama, K. *Chemical Physics Letters* **1995,** 243, (5-6), 462-468.

4. Dimitrov, A. S.; Nagayama, K. *Langmuir* **1996,** 12, (5), 1303-1311.

5. Dujardin, E.; Ebbesen, T.; Hiura, H.; Tanigaki, K. *Science* **1994,** 265, (5180), 1850-1852.

6. Hayward, R.; Saville, D.; Aksay, I. *Nature* **2000,** 404, (6773), 56-59.

7. Rabani, E.; Reichman, D. R.; Geissler, P. L.; Brus, L. E. *Nature* **2003,** 426, (6964), 271-274.

8. Lipscomb, L. D.; Vichchulada, P.; Bhatt, N. P.; Zhang, Q.; Lay, M. D. *Journal of materials science* **2011**, 1-11.

9. Deegan, R. D.; Bakajin, O.; Dupont, T. F.; Huber, G.; Nagel, S. R.; Witten, T. A. *Physical Review E* **2000,** 62, (1), 756-765.

10. Hu, H.; Larson, R. G. *The Journal of Physical Chemistry B* **2006,** 110, (14), 7090-7094.

11. Shen, X.; Ho, C. M.; Wong, T. S. *The Journal of Physical Chemistry B* **2010,** 114, (16), 5269-5274.

12. Horcas, I.; Fernandez, R.; Gomez-Rodriguez, J.; Colchero, J.; G√≥mez-Herrero, J.; Baro, A. *Review of Scientific Instruments* **2007,** 78, 013705.

13. Still, T.; Yunker, P. J.; Yodh, A. G. *Langmuir* **2012,** 28, (11), 4984-4988.

14. Layani, M.; Gruchko, M.; Milo, O.; Balberg, I.; Azulay, D.; Magdassi, S. *ACS nano* **2009,** 3, (11), 3537-3542.

CHAPTER 4

COMPARISON OF SELF-ASSEMBLED MONOLAYERS ON SWNT NETWORKS IN AMBIENT CONDITIONS[3]

[3] Stanley, D.M. and M.D. Lay. To be submitted in J. Mat. Sci.

4.1 Abstract Conductive SWNT thin films were made by a simple method that took advantage of coffee-ring deposition. Pristine SWNTs were processed into a solution to create these 2-dimensional (2D) films. The efficacy of this deposition was determined on the 2D SWNT network formation and connections between these networks. Hydrophobicity of the Si wafer due to vinyl silanes, 3APTES and OTMS, can manipulate the contact angles between the surface and SWNT solution. The starting SWNT concentrations do not affect the amount of order in the networks or connection since to SDS concentration was within the critical micelle concentration. Such parameters were used to make devices using a mask and double ring. Moreover, this method may be used as a pattern for encircling ringlets that can be left as individual rings or linked massive networks together.

4.2 Introduction Carbon nanotubes are one of the most studied materials due to its physical and electrical properties. They can be applied in vast number of fields including sensors, LEDs, and transistors. In particularly, SWNTs have shown the potential to replace current materials in such fields. However, a method that would use their properties is still not clearly defined. Developing SWNT networks involves the challenge of control and ease during growth of the network. Thus, using solution-based processing to disperse SWNTs has been proven effective to provide pristine tubes with high-aspect ratios that are ready for deposition.

Addressing issue of controlled deposition requires an evaluation of the growth of the SWNT networks. Manipulating formation of these networks, the order of the network and as well as the connection between networks are good references to compare the routes of the growth rate and direction. There have been examples that use growth of the

particles during a deposition. The strong interaction between the functionalized silane and SWNTs greatly determines the alignment and density of SWNTs due to the charge of the silane and its functionalized patterns created on the substrate. Thus, a significant degree of control in deposition of individual nanotubes at specific locations on a surface is the start for SWNT networks.

In the past couple of years, the development from our group is that the coffee-ring (CR) phenomenon may be an alternative to create random 2D SWNT networks than using only convective flow.[1] Several articles have reported the creation of networks and then connection of them with each other randomly.[2-4] Atomic force microscopy images demonstrated the ease and capability of this phenomenon; however, in order to functionalize these connected networks arbitrarily, there are a few qualifications. Though a great deal of control on their formation is highly desirable, the disorderly placement of SWNTs is what gives its abilities for different applications.[5] Thus, finding a reliable method for 2D SWNT network deposition needs to be approached.

Using CR patterning provides a simple way to modify devices of a surface in order to alter roughness, reactivity, and optical properties. Moreover, the random formation of networks was forced on the edges of the droplet, and then incubation time is part of the motion of the tubes in the droplet. The ring pattern provides a way to layer the ring droplet. Different parameters have been tested in previous work that showed their influence on network formation.[6] For example, the starting concentrations have no affect on the result and humidity does affect how the tube adheres to the surface and its orientation. Developing a means to create and to link semi-ordered SWNT networks that are conductive is focused in our research recently. Forming conductive patterns at room

temperature in a single step is unmet need. In this report, the CR deposition method, a concept for incorporating SWNT solution into the conductive networks, is explored.

4.3 Experimental Methods

SWNT suspension preparation

To form suspensions of unbundled SWNTs with high-aspect ratios, a probe sonication (Branson, 250) was used to disperse as produced, arc-discharge SWNTs (Carbon Solution Inc.) in 1% sodium dodecyl sulfate solution while minimizing damage for 30 min at 12 W. Next, a low-G centrifugation process was repeated for 45 min at 18,000 G (Beckman, GS-15R) where top half of supernatant was decanted after each cycle. Afterwards, purity of these stable suspensions, verified with UV-VIS-NIR spectroscopy (Varian Cary 5000) and Raman microscopy (Thermo Fisher, DXR), was composed of 0.03 mg/mL SWNTs for depositing the networks.

Substrate preparation

Silicon wafers were cleaned with CO_2 before deposition of 10 mM (3-aminopropyl) triethoxysilane (APTES, Aldrich) in ethanol for 45 min. After incubation, water and ethanol rinsed the silane solution off the wafer and then dried with N_2 gas. Finally, CO_2 removed excess layers of APTES to yield a monolayer (Figure 4.1).

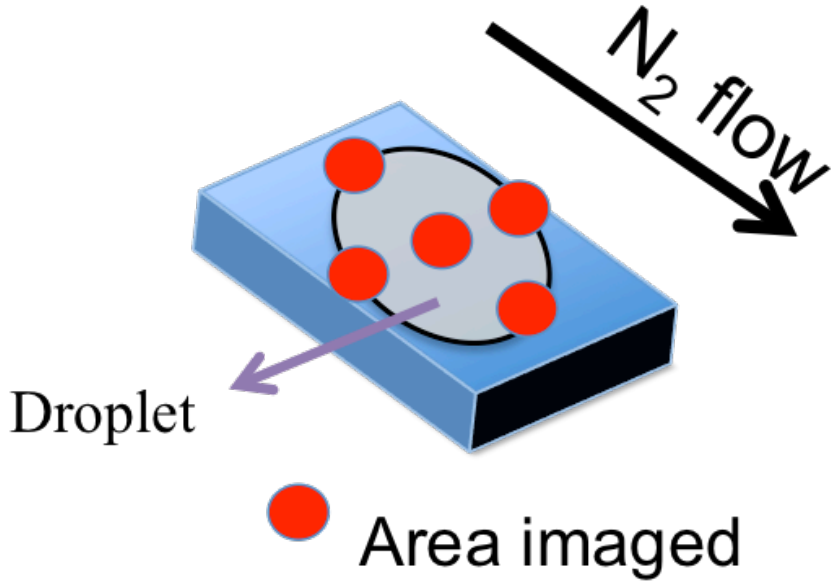

Figure 4.1. Parameters of preparation and data collection. A droplet was placed on silane-coated Si/SiO_x wafer. The direction flow of N_2 that dried the droplet and images that were taken as indicated by the red dots of the fragment are shown.

Network formation

The morphology of subsequent SWNT networks from each method was examined with intermittent mode atomic force microscopy (AFM, Pico Plus, Molecular Image). Average height from the height histograms was generated from image analysis software (WSxM v 5.3).[7] Experiments were performed under a humidity range of 27—51 %, having a median of 41 %, and temperature range of 70—80 ^{0}F, having a median of 74.4—74.7 ^{0}F. Seven volumes were chosen to compare their efficiency to control the density of SWNT networks. The volumes are 10, 20, and 30 μL. For the deposition method, a drop of the SWNT suspension was incubated on the substrate for three different times of 3 and 5 minutes. AFM scanned five images on the top, sides, and bottom of the edge as well as the center of the droplet. Later, more images were

produced to assess closely the edges of the droplet. Five images from inner, middle, and outer of each area of the edge were obtained (Figure 4.2).

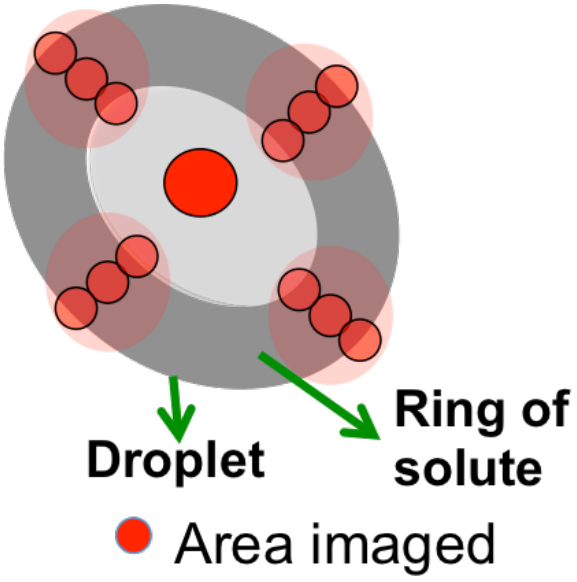

Figure 4.2. Location of Collection of AFM Images. A droplet was placed on silane-coated Si/SiO_x wafer, dried with N_2 gas, and images that were taken as indicated by the red dots of the fragment are shown above. Image of the droplet's edge is enlarged to show the sets of images taken at the outer, middle, and inner parts of the edge as well as the center of the droplet.

4.4 Results & Discussion

Comparison of silanes

To test how the surface wettability influences the SWNT density as well as the bundle formation and alignment, the CR deposition using octadecyltrimethoxysilane (OTMS) was compared to CR deposition using 3APTES. OTMS is used for preparing hydrophobic surfaces from homogeneous patterns of self-assembled monolayers.[8] This is essential for the reproducibility of electronic devices.

Similar preparation of the surface was used for the OTMS at room temperature. Based on the consistency of the droplet area and the most precise upper trend seen in the temporal studies, the volume 30 μL was chosen from the deposition trial using 3APTES for the trial using hydrophobic silane, OTMS. The desire of optimal parameters for 2D formation and SWNT density was found using that volume during 1, 3, and 5-minute incubation periods. The main focus of the experiment was consistent droplet area so not to introduce more parameters in the experiment and lowest standard deviation to give the most precise results. The only methodical deviations for each temporal trial were the relative humidity and temperature, 29 % and 77.9 °F respectively. Moreover, the temporal trials using 3APTES have a range 41 – 47 relative humidity % and 73.3 – 75.6 °F.

The different layers of the ring deposition are averaged and then, compared to 30 μL (Figure 4.3). The first and third minutes for the OTMS trials are approximately 4 nm for the average height and 2 units for the RMS roughness, which are similar averages in the outer, middle, and inner layers of the 3APTES trials. However, the averages increased in the 3APTES trial as the incubation time increased. In comparison, the inner layer of the three-minutes trial decreased using OTMS. This is due the overall decrease seen in that trial. Finally, the five-minute trial showed the most increase in both roughness and average height. Whereas the outer layer of the OTMS trial had a significant jump, the 3APTES trial increases in one-unit increment for all temporal trials.

(a)

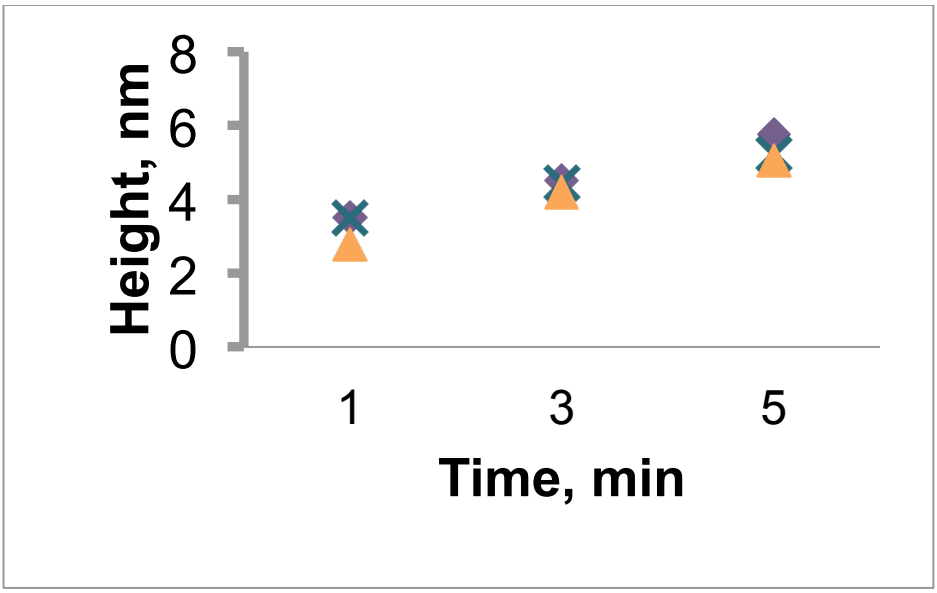

(b)

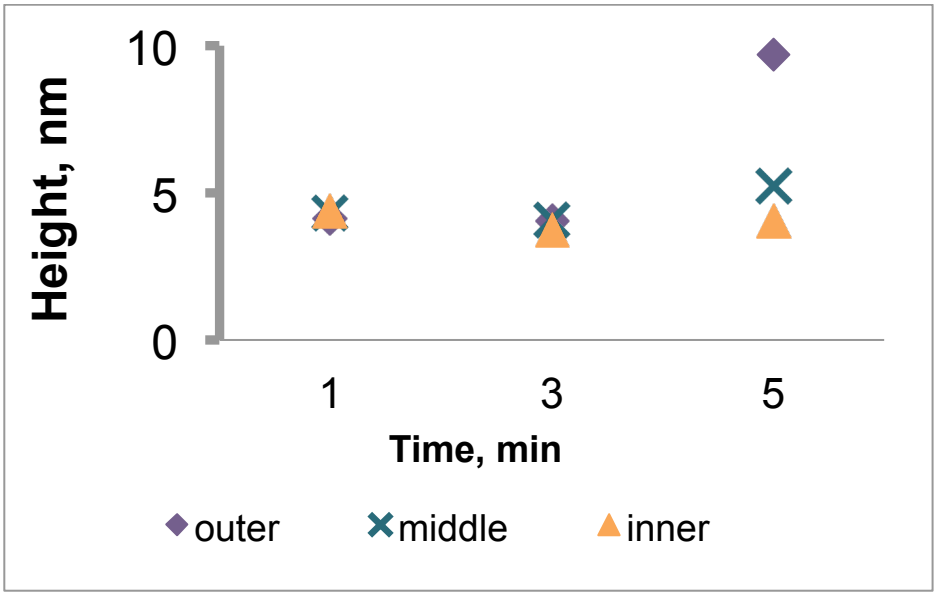

Figure 4.3. Height averages of outer, middle, and outer layers of 30 µL using 3APTES and OTMS. Comparing 30 µL using 3APTES (a) to 30 µL using OTMS (b), there is more evaporation occurring in the outer layer at 5 min for OTMS, thus more 3D bundles. Other times and layers using OTMS are similar to the 3APTES.

Examining the outer, middle, and inner layers, the 2D formations can be seen at different sides of the droplet (Figure 4.4). The difference between the silane trials is that OTMS trials show a more evenly distribution of the SWNTs than the other silane. The

top or right layer had a higher distribution of the nanotubes and impurities. Since that trend was typically seen throughout the volumetric trials using 3APTES, it can be hypothesized that ring deposition using OTMS would have a more uniformly nanotube density and quite possibly uniform 2D bundle formations throughout the ring. However, further analysis of the droplet's side would need to be investigated in order to conclude such claim. Again, the upper trend is seen as the incubation time increases, which is due to the CR effect.

The response of a droplet rolling off a surface depends largely on how the droplet interacts with the surface. This response can be quantified by contact angle hysteresis.[9] Contact angle hysteresis is the difference between the advancing and receding contact angles. It can be used to characterize a surface roughness, mobility, and heterogeneity. For Shao et al, altering the natural process of evaporation led to uneven distribution of the particles, resulting in different ring formations.[10] As previously learned, the different silanes do not change the orientation of SWNTs placed on the surface since the forces due to CR motion and laminar flow strongly affected the direction of flow.

(a) 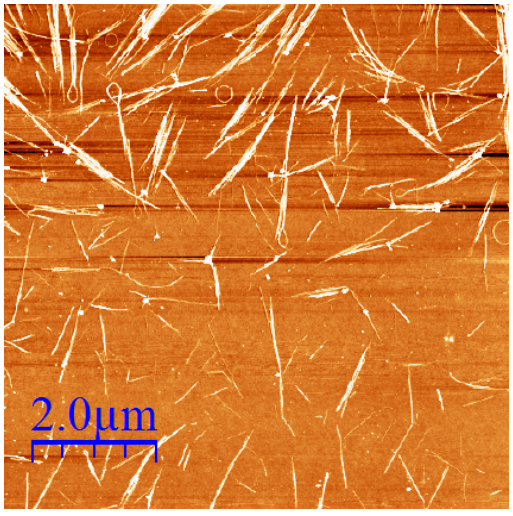

(b) 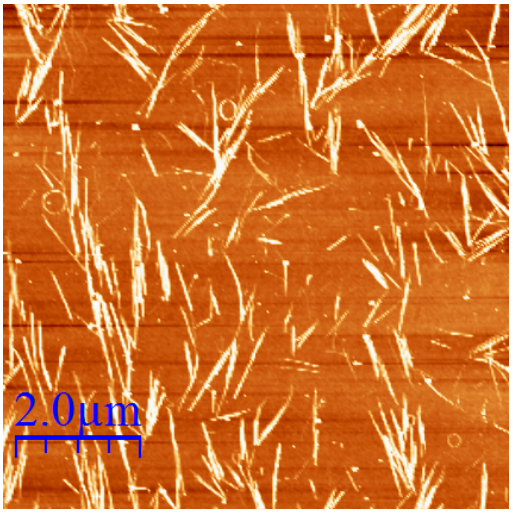

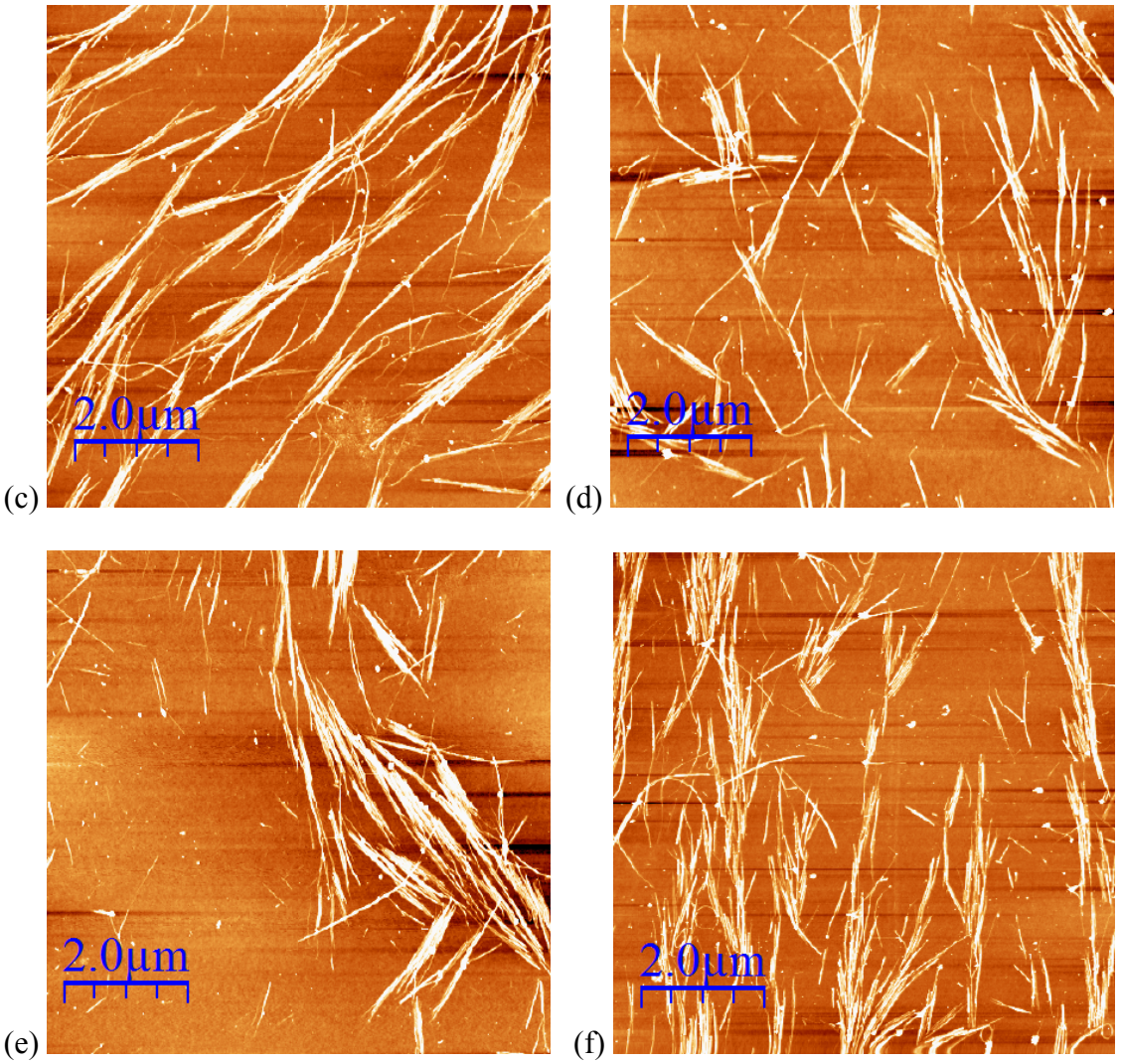

Figure 4.4. Comparison of AFM images of the ringlet of 30 μL after 3-minute deposition time using 3APTES or OTMS. (a), (c), (e) Top side of the ringlet, right side of the ringlet, and left side of the ringlet using 3APTES respectively. (b), (d), (f) Top side of the ringlet, right side of the ringlet, and left side of the ringlet using OTMS respectively. Vertical alignment and better distribution of SWNT density were more evident than ringlet that used 3APTES. Alignments and SWNT patterns differed on each side of the ringlet that used.

Different Concentrations

Different concentrations of SWNT solution were used to show that the amounts of SWNT soot have little effect on the network formation. The starting concentration determined the amount of nanotubes is in the solution; however, the tubes all get deposited on the edge of the ringlet the same. The random networks are still formed, and the time required for the network formation is the same. This suggests that there are enough nanotubes in the suspension at all three concentrations. Thus, the CRs can be made with very diluted concentration like 0.1 mg/mL up to ten times that concentration. This is interesting since the past deposition methods used by our group require higher concentration than 0.1 mg/mL and a higher number of depositions. Since the convective flow greatly influences on the orientation, the network formation can be controlled enough to form the networks, yet random positions can be created.

Less soot before the solution was processed would cause more separation between individual SWNTs and between networks when the surfactant SDS was held constant. This was caused by the SDS reduced the friction between the surface and solution, hence the CR appeared. The growth of these networks could be slowed and thus manipulation of the network direction could be attained. Yet, that idea was disproven since the same amount of order and types of formation were seen. Perhaps the SDS concentration would need to be manipulated to prove this idea.

4.5 Conclusion An account in which networks were formed from pristine SWNTs using the CR deposition was studied as a possible conventional method for SWNT 2D network formation. Observing the level of order during network formation, the changes of different silanes, concentrations, and devices were compared using AFM and 4-probe

electrical measurements. Like 3APTES, OTS provided similar amounts of network formation and connections between networks despite its hydrophobicity. Changing the starting concentration of unprocessed SWNT solution showed that there is no difference with low concentrations. Thus, higher concentrations may influence the formation since the critical micelle concentration of SDS will predict the growth rate of SWNT formation. In other words, the effect can control the level of randomness and order of the SWNT networks.

In the future, the CR deposition can simply manufacture the electrical devices rapidly was used. Firstly, the double-ring patterns may become a part of device-making procedure and replace photolithography. But for now secondly, the structure should allow multiple rings to be added and still give the similar result.[11] Probably more rings can stabilize the potential and generate current throughout the ringlet. Furthermore, further investigation of SWNT device parameters would allow a better study of the electrical behavior of the 2D SWNT networks.

4.6 References

1. Bhatt, N. P.; Vichchulada, P.; Lay, M. D. *Journal of the American Chemical Society* **2012,** 134, (22), 9352-9361.

2. Dimitrov, A. S.; Nagayama, K. *Langmuir* **1996,** 12, (5), 1303-1311.

3. Du, F.; Fischer, J. E.; Winey, K. I. *Physical Review B* **2005,** 72, (12), 121404.

4. Choi, S.-J.; Bennett, P.; Takei, K.; Wang, C.; Lo, C. C.; Javey, A.; Bokor, J. *ACS nano* **2012,** 7, (1), 798-803.

5. Bachtold, A.; Hadley, P.; Nakanishi, T.; Dekker, C. *Science* **2001,** 294, (5545), 1317-1320.

6. Stanley, D. V., P; Lay, M, Investigating Coffee-Ring Deposition Method for 2-Dimensional SWNT Network Formation. To be submitted.

7. Horcas, I.; Fernandez, R.; Gomez-Rodriguez, J.; Colchero, J.; G√≥mez-Herrero, J.; Baro, A. *Review of Scientific Instruments* **2007,** 78, 013705.

8. Ressier, L.; Viallet, B.; Grisolia, J.; Peyrade, J. P. *Ultramicroscopy* **2007,** 107, (10–11), 980-984.

9. Quéré, D. *Physica A: Statistical Mechanics and its Applications* **2002,** 313, (1), 32-46.

10. Shao, F. F.; Neild, A.; Alan, T. *Colloids and Surfaces A: Physicochemical and Engineering Aspects* **2012,** 398, 64-68.

11. Layani, M.; Gruchko, M.; Milo, O.; Balberg, I.; Azulay, D.; Magdassi, S. *ACS nano* **2009,** 3, (11), 3537-3542.

CHAPTER 5

CONCLUSION AND FUTURE WORKS

5.1 Conclusion Since its discovery in 1991, carbon nanotubes have created new boundaries for the chemistry of the carbon. In particularly, this dissertation has been focused on the control and manipulation of SWNT properties for various applications. The formation of SWNT networks is an important part of manufacturability, and a method that placed these tubes into a liquid phase has been used. It supports the main goal that is to predict the placement of SWNTs. Hence, this has the potential of improving electron transfer and making them more accessible for further process. In general, SWNTs were purified and suspended into individual tubes with high-aspect ratios. This process was detected and characterized by different spectroscopic and probing techniques.

A couple of protocols for the formation of SWNT networks have been proposed. As in the case of network formation, the determination of a given method would depend on the purpose for the system. For example, some may prefer the immerse method since it provided plenty of networks that were more evenly distributed from the point of view of large-scale production, while others like the drop method because it decreases the amount of impurities on the surface and creates a platform for further modifications.

Furthermore, much work is needed still towards the manufacturability of CNT-based electronics. Yet, the combination of the unique properties of SWNTs and known advantages of the deposition techniques represents a very good alternative for the

development of SWNT-based devices that are capable to address the technological challenges of the future.

5.2 Future Works Expanding the current study, the search for the optimal concentration of SWNT suspensions that enables a uniform deposition and consequently predicting the electrical properties of 2D SWNT networks is of great interest. As stated earlier, the effects of the different diameters of the droplet manipulated the homogeneity of the CR ringlet. In addition, the diameter of ringlets could be more significant throughout the deposition process. Yet, this is a current assumption, and the idea to form 2D networks would require the knowledge of the internal behavior of the suspension. Even though evaporation is only occurring in a period of 1, 3, or 5 minutes, the change in diameter during incubation would impact the internal flow motion. To evaluate this assumption, monitoring the incubation time to compute the droplet diameter and contact angle at all times. Also, another study would continue the comparison of SWNT/substrate interactions as a function of various head groups of silane using spectroscopic and probing techniques.

Finally, the preliminary work described below addresses the groundwork for very relevant studies. Table 5.1 indicates that the degree of semiconducting behavior of SWNT networks after linkage of two rings that were formed from the drop method described previously. The setup as shown in Figure 5.1 used the double-ring pattern to form electrodes. The wafer substrate was functionalized with 3APTES. 30 μL of SWNT solution of 0.03 mg/mL based on absorbance of solutions without centrifugation performed was deposited onto the wafer substrate for an incubation time of 5 minutes. One probe was placed on the, and the other was placed inside the droplet to measure the

conductivity. Though the ratio of ON-OFF state of second ringlet device behaved more metallic than semi-conducting SWNT, this is crucial for building and connecting random networks together. Future studies include the following: AFM studies to analyze any change of morphology at the junction of the two rings, incubation studies to have different times for the looped rings to understand its effect on the second ringlet, and conductive AFM studies to map the electrical pathways of SWNT networks in order to understand further how percolation occurs in the networks.

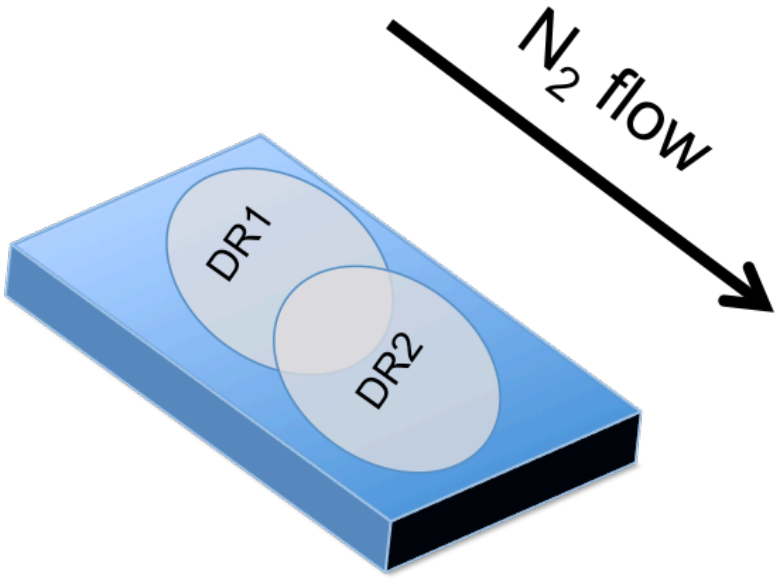

Figure 5.1. Schematic Diagram of the double-ring pattern. DR1 is the first ring deposited. DR2 is the second ring deposited. Electrical measurements were taken from the ringlet of DR2 due to more connectivity than DR1.

Table 5.1. ON-OFF Ratios of the Second Ring of the Double-Ringed Pattern

Section of the 2nd Ring	ON-OFF
Top	3.3±0.7
Right	2.2±0.4
Bottom	1.8
Top-Right	2.0±0.8